The effect of external electric fields on biological systems: theoretical-computational study

Ambra Tarquini

Supervisori:
Prof. Alfredo Di Nola   Ottobre 2009
Dr. Andrea Amadei

The effect of external electric fields on biological systems: theoretical-computational study

Ambra Tarquini

Supervisori:
Prof. Alfredo Di Nola   Ottobre 2009
Dr. Andrea Amadei

CONTENTS

*Imagination is more important than knowledge. For knowledge is limited to all
we now know and understand, while imagination embraces the entire world, and
all there ever will be to know and understand!*

Albert Einstein

This Thesis is based on the following pubblications:

1. A. Tarquini, A. Amadei and A. Di Nola
Theoretical and computational characterization of dilute ionic solutions under the effects of external electric field
Biophysics and Bioengineering Letters 1(1), 1-8 (2008).

2. A. Tarquini, P. Marracino, F. Apollonio, M. Liberti, G. d'Inzeo, A. Amadei and A. Di Nola
Theoretical and computational characterization of the thermodynamic effects of external electric fields in dilute ionic solutions
IJLSS, Accepted (2009).

ONE

INTRODUCTION

The electric field effects in biological systems are of long-standing scientific interest. The fact that electrical currents can affect the behavior of biological systems has been known for more than 2000 years, and electric shocks have been used to treat a wide variety of ailments off and on ever since.[1] However, it is surprising how incomplete our knowledge is today of the effects of direct current and low frequency voltages and currents on biological systems. Electrical signals are clearly important in the control of biological processes and in carrying information from one part of the body to another. Nerve cells propagate electrical signals from sensors of pressure, temperature, light, sound, etc., to the brain and return control signals to muscles and other tissue.

Purpose of the description of basic interactions between biological cells and electric fields is the understanding of specifying the general level or intensity of fields, currents, temperatures where one can expect to observe a given class of biological responses.[2] Biological cells consist of complex physical subsystems. In an attempt to understand them, the most elementary level will be described. Perhaps the simplest level, which is already surprisingly complicated, is the effect of electric fields on biological fluids. These fluids contain a large number of components, including ions, polar molecules such as water, proteins, lipids, hormones and colloidal particles. Current flow in these fluids is given by the sum of the drift and diffusion currents for each component.

The next level of complexity involves the interaction of the fields with mem-

branes that behave like porous solids for fields applied perpendicularly to their surface, and like viscous liquids for fields in the plane of the membrane.[3] Membranes are inhomogeneous so that different portions of them may be affected differently by the perturbing fields. Additionally, membranes are involved in active chemical reactions that change their porosity to various ions selectively, so that both electrical potentials and chemical signs may change the membrane's conductivity by orders of magnitude.

Electric fields affect the selective transport of ions or molecules through the membrane.[4] They change the build up of charged ion layers at the surface and change the way new molecules are incorporated into the membrane or are bound to its surface. Changes in the transport of molecules or ions across cell membranes affect the performance of the cells and, in turn, of the organs of which they are a part. For example, electric fields applied to the myocardium tissues, can modify the frequency of discharge and so of the heartbeat and of the cardiac output. Therefore, at the macromolecular level of the biological scale of complexity, the cellular membrane and its substructures, such as receptors and ion channels, have been identified as the most plausible target of interaction. Their shape, charge or energy may be altered under exposure to exogenous electric fields, hence triggering a chain of events that ultimate in a macroscopic observable effect. Although the huge number of both theoretical and experimental investigations performed over the years, at present the mechanisms at the basis of specific field-induced effects are still not completely known and understood.

In this wide scenario, one of the purposes of this research activity is to study the thermodynamic characterization of liquid water, ionic solutions under the effect of an external (static) electric fields through both theoretical and computational methods. There are several situations in which H-bonding molecules are subject to electric fields, such as in the electrical double layer, around ionic species and in externally applied electric fields. They influence many phenomena, such as gatting of biological ion channels, solvation dynamics and folding of proteins. Understanding of the behavior of H bonds in the presence of electric fields is an important area of research.

There are some relevant theoretical studies of homogeneous H-bonded fluids not subject to external electric field that are listed in succession. Stanley and Teixeira[5] used a simple correlated-site percolation theory to study the dependence

of various dynamical and thermodynamical properties of water systems against temperature and pressure variations, the dilution with D_2O and the presence of impurities. They obtained an expression for the distribution of water molecules as a function of the number bonds to be a binomial distribution, and their results were in excellent agreement with experimental data and computer simulations.

Sastry et al.[6, 7] studied the thermodynamics of the supercooled water introducing a lattice model which does not exhibit any low temperature singular feature. The model assumes that each lattice cell can have its volume changed if hydrogen bonds are taken into account. Their results captured qualitatively the thermodynamical properties of the cooled water, and showed that the increase in compressibility upon lowering temperature is not related to any singular behavior.

Suresh[8] proposed a new lattice-based, mean-field theory for predicting alignment of molecular dipoles and hydrogen bonds in liquids subject to uniform electric fields. This theory was applied to understand the internal structure of hydrogen cyanide in the liquid state at different electric fields. They have found that electric field influences the internal structure of H-bonding fluids in a complex manner. Electric field induces dipolar alignment, which in turn influences the bonding patterns.

With the availability of large scale computers, Monte Carlo (MC) and Molecular Dynamics (MD) simulations have been introduced and developed as powerful methods to understand systems, such as the water, on a molecular level.

Several key aspects, such as, data concerning structural and dynamical properties of water and aqueous solutions, were revealed by MD simulations.

Two main results from the computer simulations of a chloride ion in water under an applied external electrical field have been shown[9]: i) An enhancement of the water structure with increasing strength of the electrical field has been deduced from radial distribution functions, hydrogen bond distributions and tetrahedrality deviations. ii) The self-diffusion coefficient decreases strongly with increasing strength of the external electrical field as a consequence of the increased structure.

Simulations with the rigid TIP4P water model, with MD method, have been used to investigate the structural change of liquid water induced under an external electric field.[10] It resulted an enhanced structural regularity generated by the electric field in the process of simulations instead of obtaining solidified water. Application of an external static electric fields to small water cluster[11] induces sig-

nificant structural and dynamic changes in a nonmonotonic way. These changes affect the reactivity and solvation capacity of the cluster. MD simulations were also used to study the influence of an external uniform electrostatic field on the internal energy and polarization of a medium-sized water cluster, consisting of 40 molecules, at four temperatures.[12] The system showed an abrupt change of its properties at some critical value of the field, where a transition from a normal to a superpolarized cluster state is observed. MD investigations[13] at 258K of liquid water, as a function of different strengths of an external electric field, and by employing the flexible simple point charge model (SPC), showed an enhancement of the water hydrogen bond structure with increasing strength of the electric field. With increasing field strenght, water system has a more perfect structure, which is similar to ice structure.

Despite these extensive theoretical studies, direct experimental measurements are sparse. Recently, using X-ray scattering, Toney et al.[14] measured the water density profile perpendicular to a silver (111) surface at two applied voltages. They found that the water molecules are ordered in layers extending about three molecular diameters from the electrode, and that the spacing between the electrode and first water layer indicates an oxygen-up (oxygen-down) average orientation for negative (positive) charge. Moreover, they also found that the first layer has a far greater density than that in bulk water. This implies that the hydrogen-bonding network is disrupted in this layer, and that the properties of the water in the layer are likely to be very different from those in the bulk. In another study,[15] the same authors, using surface X-ray scattering, confirmed that the molecular water arrangements in the inner layer are significantly different from bulk, due to the strong electric field at the charged Ag(111) electrode.

In the present study, the characterization of the thermodynamic effects of external electric fields in dilute ionic solution has been investigated by the combined use of the quasi-Gaussian entropy theory and molecular dynamics simulations. Principally, the thermodynamic variations induced by the applied electric field may be very important, not only to understand the response of a complex system like a liquid exposed to an external field, but also to obtain fundamental informations for manufacturing and designing nano-technological devices.

Another purpose of the present thesis is the MD simulations of micelles under the effect of a static external electric field.

Numerous experimental and theoretical studies have been carried out to determine the nature of their structure and dynamics. Interpretation of experimental results is often model dependent making theoretical studies of micelles relevant in order to obtain a molecular interpretation of experimental observables.

Theoretical approaches, initially applied to micelles, employed lattice-based chain models.[16, 17] With increased computational resources, MD simulations have recently been used, allowing for a more detailed microscopic understanding of the micellar properties to be obtained.[18, 19] MD studies have been performed on a variety of systems, including dodecyl surfactants, sodium octoanate, lysophosphatidylethanolamine, and n-decyltrimethylammonium chloride, in environments ranging from vacuum to fully solvated with counterions in the presence of periodic boundary conditions. For zwitterionic micelles, a short simulation of micelle lysophosphatidylethanolamine[20] and a 1.2-ns simulation of a dodecylphosphocholine micelle are available.[21]

Simulations of dodecylphosphocholine (DPC) micelles of three different sizes (40, 54 and 65 lipids) in water for up to 15 ns have been reported.[22] They were analyzed in terms of energetics, structure of the water/lipid interface, structure and dynamics of the lipid tails and overall size and shape of the micelles.

Micelles have been also exploited in experimental studies, due to their potential as a model system for membrane bilayers. In fact, micelles are used as surrogates for membranes because measurements of complexed peptides, proteins, or other organic molecules are often more tractable than with bilayers. In recent years, polymeric micelles have been the object of growing scientific attention. They have emerged as a potential carrier for poorly water soluble drugs because they can solublilize those drugs in their inner core.[23]

In the specific context of drug delivery mehods, another goal of the present investigation is the characterization of the thermodynamic effects of external electric fields in micelles, using MD simulations. In particular the structural properties of the micelle are studied and the effects induced by homogeneous electric field are underlined

The thesis is organized as follows: in **Chapter 2** will be described the method computational used, Molecular Dynamics (MD), that is a sampling method of the phace space where the dynamic behavior of the system is investigated evolving the Newton's second law equation in a proper statistical ensemble.

In **Chapter 3** will be described the quasi-Gaussian entropy theory (QGE) where the basic statistical mechanical relations are rewritten in terms of the distribution of the fluctuations of a macroscopic property instead of the partition function.

In **Chapter 4**, the theoretical and computational characterization of the thermodynamic effects of external electric fields in dilute ionic solutiond are reported.

In **Chapter 5**, the structural characterization of a water-micelle system under the effect of external electric fields by the use of MD simulations are discussed.

TWO

MOLECULAR DYNAMICS SIMULATIONS

2.1 Introduction

Some basic concept and methodologies of molecular simulations are introduced here, with a particular attention devoted to the methods relevant to this thesis. For further readings on these subjects, several books can be found with a deeper insight into MD techniques [24, 25, 26]. As the method used in the present thesis to study the properties of dilute ionic solutions by the external electric field, is classical Molecular Dynamics (MD, a brief description of its basic principles is presented.

2.2 Classical Molecular Dynamics

The aim of computer simulations of molecular systems is to compute macroscopic behavior from microscopic interactions. A model of the real world is constructed, both measurable and unmeasurable properties are computed and the former are compared with experimentally determined properties. If the model used is validated by the comparison, it could even be used to predict unknown or unmeasurable quantities. A theoretical treatment of the motions and interactions of molecules should be founded, rigorously speaking, on quantum mechanics principles, due to the microscopic nature of these objects. Unfortunately, first-principle approaches are often unpractical because they require very large computational

facilities and they are definitely prohibitive for systems containing thousands of atoms. Hence, a certain level of approximation becomes necessary and it should be chosen in such a way that those degrees of freedom that are essential to a proper evaluation of the quantity or property of interest can be sufficiently sampled. When excluding chemical reactions, low temperatures or details of hydrogen atoms motion, it is relatively safe to assume that the system is governed by the laws of classical mechanics.

In classical MD, a trajectory (configurations as a function of time) of the molecular system is generated by simultaneous integration of Newton's equations of motions for all atoms in the system:

$$\frac{d^2\mathbf{r}_i}{dt^2} = m_i^{-1}\mathbf{F}_i \qquad (2.1)$$

$$\mathbf{F}_i = -\frac{\partial V(\mathbf{r}_1, \ldots, \mathbf{r}_N)}{\partial \mathbf{r}_i} \qquad (2.2)$$

The force acting on atom i is denoted by $\mathbf{F}_i$, the mass by m_i and time is denoted by t. MD simulations require calculation of the gradient of the potential energy $V(\mathbf{r}_1, \ldots, \mathbf{r}_N)$, which therefore must be a differentiable function of the atomic coordinates $\mathbf{r}_i$. This potential energy function, or *force field*, is called an *effective interaction* function since the average effect of the omitted (electronic) degrees of freedom has been incorporated in the interaction between the (atomic) degrees of freedom explicitly present in the model.

The choice of molecular model and force field is essential to a proper prediction of the properties of a system. Therefore, it is of great importance to be aware of the fundamental assumptions, simplifications and approximations that are implicit in the various types of models used in the literature.

2.2.1   Force Field Models

A huge variety of force fields is currently used in the molecular dynamics community, sometimes differing for minor changes, e.g. CHARMM,[27] AMBER,[28] GROMOS.[29] A typical molecular force field, or effective potential, for a system of N atoms with masses m_i ($i = 1, 2, \ldots, N$) and Cartesian position vectors $\mathbf{r}_i$ has the following form:

$$V(\mathbf{r}_1, \mathbf{r}_2, \ldots, \mathbf{r}_N) = \sum_{bonds} \frac{1}{2} K_b (b - b_{eq})^2 + \sum_{angles} \frac{1}{2} K_\theta (\theta - \theta_{eq})^2$$

$$+ \sum_{dihedrals} K_\phi [1 + cos(n\phi - \delta)] + \sum_{imp.dihedrals} \frac{1}{2} K_\xi (\xi - \xi_{eq})^2$$

$$+ \sum_{pairs} 4\epsilon_{ij} \left[\left(\frac{\sigma_{ij}}{r_{ij}} \right)^{12} - \left(\frac{\sigma_{ij}}{r_{ij}} \right)^6 \right] + \sum_{pairs} \frac{q_i q_j}{4\pi\epsilon_0 r_{ij}} \qquad (2.3)$$

The first term represents the covalent bond stretching interaction between two atoms linked by a harmonic potential where b_{eq} is the minimum energy bond length and K_b is the force constant changing with the particular bond type. The second term is a three-body interaction corresponding to the valence angle, θ, deformation expressed as a harmonic potential where θ_{eq} is the equilibrium valence angle and K_θ the force constant. The third and fourth terms are used for the (four-body) dihedral angle interactions: a harmonic term for improper dihedral angles, ξ, that are not allowed to make transitions, i.e. to keep the aromatic rings planar, and a sinusoidal term for all the other dihedral angles, ϕ. The last two terms are sums over the pairs of non-bonded atoms and represent the effective non-bonded interactions expressed in terms of van der Waals and Coulombic interactions between atoms i and j at a distance r_{ij}. The parameters ϵ_{ij} and σ_{ij} are the typical constants defining the Lennard-Jones potential, q_i and q_j are the atom charges and ϵ_0 is the dielectric constant in vacuum.

The parameters used in the force field (Eq. 2.3) can be determined in different ways. Generally two main approaches are followed. The first one is to fit them with results obtained from *ab initio* calculations on small molecular clusters. The alternative way is to fit the force field parameters to experimental data, like crystal structures, energy and lattice dynamics, infrared or X-ray data on small molecules, liquid properties like density and enthalpy of vaporization, free energy of solvation, nuclear magnetic resonance data, etc. Whatever method is used, the resulting model is far to be universal. It is worth to note that every force field is usually well suited for specific general conditions, i.e. particular thermodynamic conditions (temperature, density, pressure, etc.) and also boundary conditions. Moreover, they are optimized for specific classes of molecules, such as inorganic molecules,

organic molecules, biomolecules (DNA, proteins, lipids), etc.

2.2.2 The Boundary Conditions

An important characteristic of the molecular dynamics simulations is the way in which the boundaries are treated. Due to computational limits, a typical simulated system contains $10^4 - 10^5$ atoms, and then is quite small compared to macroscopic matter. This means that, if the molecules are arranged in a cubic box, a relatively great part of them will lie on the surface and will experience quite different forces from molecules in the bulk. The consequence of the finite size of the system is that the boundary conditions may affect seriously the results of the simulations, especially when the system of interest is a homogeneous liquid or a solution. Usually, periodic boundary conditions (PBC) [24] are adopted to reduce the surface effects. This technique consists on simulating the system in a central cubic box surrounded by an infinite number of copies of itself. During the simulation, the molecules in the original box and their periodic images move exactly in the same way. Hence, when a molecule leaves the central box one of its images will enter through the opposite side. As a result, there are no physical boundaries neither surface molecules. Note that other shapes of the box can be used as the truncated octahedron or the rhombic dodecahedron.

2.2.3 Integration of Motion Equations

Newton's equations of motion, a second-order differential equation, can be written as two first-order differential equations for the particle positions $\mathbf{r}_i(t)$ and velocities $\mathbf{v}_i(t)$ respectively:

$$\frac{d\mathbf{v}_i(t)}{dt} = m_i^{-1}\mathbf{F}_i \qquad (2.4)$$

$$\frac{d\mathbf{r}_i(t)}{dt} = \mathbf{v}_i(t) \qquad (2.5)$$

A standard method for solution of the previous ordinary differential equations is the finite difference approach. The general idea is the following. Given the molecular positions, velocities and forces at time t, we attempt to obtain the

positions, velocities and forces at a later time $t + \delta t$, to a sufficient degree of accuracy. The equations are solved on a step-by-step basis; the choice of the time interval δt will depend somewhat on the method of solution, but δt will be significantly smaller than the typical time taken for a molecule to travel its own length.

Many different algorithms fall into the general finite difference pattern, like Verlet, and its computational efficient variant *leap-frog*,[30, 31] Beeman [32] or the Gear predictor-corrector.[33]

2.2.4   Enhanced efficiency methods

Since the first published application of MD to biomolecular systems,[34] a little more than 20 years ago, people have devised methods to increase the time scales of MD simulations. When Newton's equations of motion are integrated, the limiting factor that determines the time step that can be taken is the highest frequency that occurs in the system. In solvated biological macromolecules, the vibrations of bonds involving hydrogen atoms form the highest frequency vibrations. The bond stretching frequency of an O-H bond is typically about 10^4 Hz, so the average period would be of the order of 10 fs.[35] This limits the time-step to be taken in MD simulations to about 0.5 fs (a rule of thumb exists that states that for a reasonable sampling of a periodic function, samples should be taken at least twenty times per period). The introduction of a method to constrain these bonds (or, in fact, all covalent bonds) allowed to increase the time step to a typical value of 2 fs (*SHAKE*).[36] Since these bond vibrations are practically uncoupled from all other vibrations in the system, constraining them does not notably alter the rest of the dynamics of the system. This is not true, however, for bond-angle fluctuations, which form the second-highest frequency vibrations. Constraining bond-angles has a severe effect on many other fluctuations in the system, including even global, collective fluctuations, limiting the use of methods that use bond-angle constraints to only a few specific cases.[35]

The notion that a number of discrete classes of frequencies of fluctuations in simulations of biomolecules can be distinguished, however, can be utilized to design more efficient algorithms. Forces that fluctuate rapidly need to be recalculated at a higher frequency than those that fluctuate on a much longer time scale. Although

not trivial to implement, a number of successful applications of so-called *multiple time-step* algorithms have been reported in the literature (for a review, see Schlick *et al.* [35]). Speed up factors of 4-5 have been claimed for such methods with respect to unconstrained dynamics, making them only slightly more efficient than simulations with covalent bond-length constraints.

Another approach to reach equilibrium conformational properties at an enhanced rate is by constraining the rotational and translational motions in polyatomic systems.[37] This method is generally used to study biomolecules in solution. In such a system, the internal motions of the solute are often more interesting than its rotational and translational motions. This algorithm is implemented in a *leap-frog* integration scheme coupled with SHAKE. The use of the *roto-translational constraint* presents several advantages, like a reduction of the molecular relaxation time and the possibility of reducing the amount of solvent molecules to be used.[38]

2.2.5 Long-range Interactions

One of the most challenging problems in molecular dynamics simulations is the treatment of long-range interactions, which usually correspond to the electrostatic forces between molecules. To reduce the computational cost, the size of the simulated system is generally small and, as a consequence, a correct evaluation of the intermolecular interactions is not trivial. Many different methods were developed to reproduce reasonably the thermodynamics of bulk liquids. Here we consider two of the most used techniques: the use of a cut-off radius and the Ewald sum.

The *cut-off method* is based on the truncation of the forces when the distance between the interacting particles is greater than a specified value, called the cut-off radius, r_c. In this way, the only interactions felt by the i-th particle are those due to the particles contained in a sphere of radius r_c and centered at $\mathbf{r}_i$. This method is doable only if the intermolecular forces decay rapidly with the distance. In fact, when the forces are negligible at a distance $\geq r_c$, the main structural and dynamical properties are correctly reproduced. Otherwise deviations from the correct bulk behaviour are expected.

Another methodology in MD simulations is the use of a *periodic lattice method* in which all the interactions between the molecular system in the central cubic cell and its virtual replica are included. The Coulomb interaction energy in a periodic

system of N charged particles is obtained by a sum over all pairs of which one atom lies in the central box and the other is its periodic image:

$$E = \frac{1}{8\pi\epsilon_0} \sum_{|\mathbf{n}|=0}^{\infty} \left(\sum_{i=1}^{N} \sum_{j=1}^{N} \frac{q_i q_j}{|\mathbf{r}_{ij} + \mathbf{n}|} \right) \qquad (2.6)$$

The sum over $\mathbf{n}$ is a summation over all simple cubic lattice points $\mathbf{n} = (n_x L, n_y L, n_z L)$, with L the side length of the cubic cell and n_x, n_y, n_z integers. The case $i = j$ is omitted for $\mathbf{n} = 0$. It was shown that the sum over $\mathbf{n}$ for such kind of potential (r^{-1}) is only conditionally convergent, then its limit may vary or even diverge if the order of terms in the sum is changed. A solution to this problem was developed following a physical idea:[24] each point charge is surrounded by a charge distribution of equal magnitude and opposite sign, which spreads out radially from the charge, $\rho^G(\mathbf{r})$. This distribution has the effect to screen the interactions between the neighbouring point charges and hence the interaction energy becomes short-ranged. Commonly, the screening charges have a Gaussian form. The total charge distribution is given by:

$$\rho_i(\mathbf{r}) = \rho_i^q(\mathbf{r}) + \rho_i^G(\mathbf{r}) \qquad (2.7)$$

where $\rho_i^q(\mathbf{r})$ is the distribution of the point charge of the i-th particle and $\rho_i^G(\mathbf{r})$ is the corresponding Gaussian distribution.

First, the interaction energy due to the distribution 2.7 is calculated in the real space, then, in order to recover the original charge distribution, a canceling function is added in the reciprocal space, which is equal to $-\rho_i^G(\mathbf{r})$, realized by means of a Fourier transform. Hence the final form of the total interaction energy is given by:

$$
\begin{aligned}
E \;=\; & \frac{1}{8\pi\epsilon_0} \sum_{i=1}^{N} \sum_{j=1}^{N} \left(\sum_{|\mathbf{n}|=0}^{\infty} \frac{q_i q_j\, erfc(\alpha|\mathbf{r}_{ij}+\mathbf{n}|)}{|\mathbf{r}_{ij}+\mathbf{n}|} \right. \\
& + \left. \frac{1}{\pi L^3} \sum_{\mathbf{k}\neq 0} \frac{4\pi^2 q_i q_j}{k^2} \exp(-k^2/4\alpha^2) \cos(\mathbf{k}\cdot\mathbf{r}_{ij}) \right) \\
& - \frac{\alpha}{4\pi^{3/2}\epsilon_0} \sum_{i=1}^{N} q_i^2 + \frac{|\sum_{i=1}^{N} q_i \mathbf{r}_i|^2}{2\epsilon_0 L^3 (2\epsilon' + 1)}
\end{aligned}
\qquad (2.8)
$$

Here $erfc(x)$ is the complementary error function, which falls to zero with increasing its argument. Thus, if the parameter α is large enough, the sum over $\mathbf{n}$ in the first term reduces to the only term $\mathbf{n} = 0$. The second term is a sum over the reciprocal vectors $\mathbf{k} = 2\pi\mathbf{n}/L$. Again, if α is large, a lot of terms in the k-space sum are needed to get a convergence of the energy. The last two terms are, respectively, a correction function, due to the fact that a self-interaction of the canceling distribution is included in the recipe, and the energy contribution of the depolarizing field, which is compensated by the effect of the external dielectrics. Note that in the Ewald sum the virtual cubic cells are ordered as concentric spherical layers starting from the central box. Clearly the infinite sum is truncated at a certain point and the resulting spherical system is immersed in a continuum dielectrics with dielectric constant ϵ'. The last term in equation 2.8 is the sum of the contributions of the depolarizing field and the reaction field due to the external dielectrics. If the sphere is embedded in a medium with an infinite dielectric constant, this term vanishes because of a perfect compensation of the two effects.

Other *periodic lattice methods* are often used in computer simulations for their computational stability and efficiency. These methods, like the Particle Mesh Ewald (PME)[39] method, can be considered of the same family of the method shown here.

2.2.6   Constant Temperature/Constant Pressure Molecular Dynamics

When Newton's equations of motion are integrated the total energy is conserved (adiabatic system) and if the volume is held constant the simulation will gen-

erate a microcanonical ensemble (NVE). However, this is not always very convenient. Other statistical ensembles, such as canonical (NVT) and isothermal-isobaric (NPT) ensembles, better represent the conditions under which experiments are performed than the standard microcanonical ensemble. Moreover, with the automatic control of temperature and/or pressure, slow temperature drifts that are an unavoidable result of force truncation errors are corrected and also rapid transitions to new desired conditions of temperature and pressure are more easily accomplished.

Several methods for performing MD at constant temperature have been proposed, ranging from *ad hoc* rescaling of atomic velocities in order to adjust the temperature, to consistent formulation in terms of modified equations of motion that force the dynamics to follow the desired temperature constraint. The three most utilized methods are described next.

The *termal bath coupling* method, or Berendsen coupling,[40] has the great advantage of being simple. This algorithm simulates a coupling of the system with an external termal bath at the temperature T_0 and the interaction between this bath and the system is modulated by a time constant τ. The coupling is obtained multiplying for a constant λ the velocities. The temperature T is scaled to the reference temperature T_0 via an exponential law.

The *isothermal* , or isogaussian, method [41] allows to fix the temperature exactly constant. Using this algorithm, a variable is added to the motion equations, acting as a friction coefficient changing in time in order to keep the kinetic energy constant. This method correctly generates the configurational properties of the canonical ensemble, while the momenta distribution is not canonical.[37] *Nosé-Hoover thermostat* is based on the use of an extended Lagrangian, i.e. a Lagrangian that contains additional, artificial coordinates and velocities.[42, 43] The conventional Nosé-Hoover algorithm only generates the correct distribution if there is a single constant of motion. Normally, the total energy, that includes the artificial variables, is always conserved. This implies that one should not have any other conserved quantity. If we have more than one conservation law, we have to use the Nosé-Hoover chains to obtain correct canonical distribution.[44]

The various methods for carrying out MD at constant pressure are based on the same principles as the constant temperature scheme with the role of the temperature played by the pressure and the role of the atomic velocities played by the

atomic positions.

2.2.7   Essential Dynamics

The Essential Dynamics (ED) analysis is a method to seek those collective degrees of freedom that best approximate the total amount of fluctuation of a dynamical system.[45, 46] A brief description will be given here. ED is based on a principal component analysis (PCA) of (MD generated) structures. A PCA is a multidimensional linear least squares fit procedure. To understand how this is applicable to protein dynamics, the usual three-dimensional (3D) Cartesian space to represent protein coordinates (which is e.g. used to represent protein conformations in the Brookhaven Protein Data Bank or PDB) needs to be replaced by another, multi-dimensional space. A molecule of N particles can be represented by N points in 3D space. With 3 coordinates per point, this adds up to 3N coordinates. In a 3N-dimensional space, however, such a structure can be represented by a single point. In this space, this point is characterized by 3N coordinates. This representation is convenient since a collection or trajectory of structures can now be regarded as a cloud of points. Like in the case of a two-dimensional cloud of points, also in more dimensions, always one line exists that best fits all points. As illustrated for a two-dimensional example (Figure 2.1), if such a line fits the data well, the data can be approximated by only the position along that line, neglecting the position in the other direction. If this line is chosen as coordinate axis, then the position of a point can be represented by a single coordinate. In more dimensions the procedure works similarly, with the only difference that one is not just interested in the line that fits the data best, but also in the line that fits the data second-best, third best, and so on (the principal components). These directions together span a plane, or space, and the subspace responsible for the majority of the fluctuations has been referred to as the 'essential subspace'. Applications of such a multidimensional fit procedure on protein configurations from MD simulations of several proteins has proven that typically the ten to twenty principal components are responsible for 90% of the fluctuations of a protein.[51−53] These principal components correspond to collective coordinates, containing contributions from every atom of the (protein) molecule. Summarised, a limited number of collective motions is responsible for a large percentage of a protein conformational fluctuations.
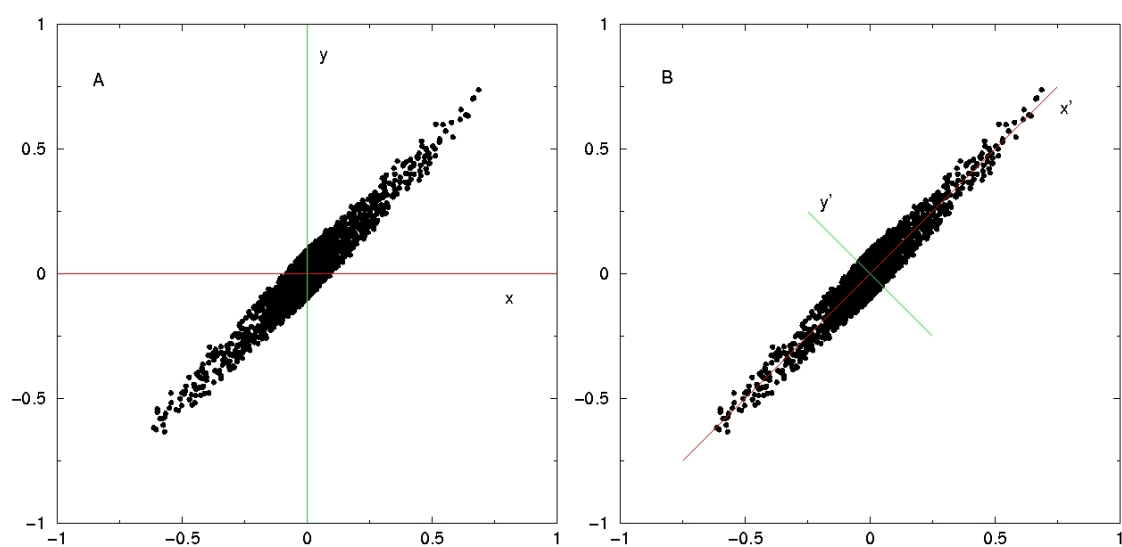
Figure 2.1: Example of Essential Dynamics in two dimensions. With a distribution of points as depicted here, two coordinates (x,y) are required to identify a point in the cluster in panel A, whereas one coordinate (x') approximately identifies a point in panel B

If all atoms in a protein were able to move uncorrelated from each other, an approximation of the total fluctuation by only a few collective coordinates would not be possible. The fact that such an approximation is successful is the result of the presence of a large number of internal constraints and restrictions ('near-constraints') defined by the interactions present in a given protein structure. Atomic interactions, ranging from covalent bonds (the tightest interactions) to weak non-bonded interactions, together with the dense packing of atoms in native-state protein structures form the basis of these restrictions.

In the study of protein dynamics, only internal fluctuations are usually of interest. Therefore, the first step in an Essential Dynamics analysis is to remove overall rotation and translation. This is done by translation of the center of mass of every configuration to the origin after which a least squares rotational fit of the atoms is performed onto to a reference structure. The actual principal component analysis is based on construction and diagonalisation of the covariance matrix of positional fluctuations. Defining the 3N dimension column vector $\mathbf{X}(t)$ representing the atomic coordinates of the system at time t, the covariance matrix is built up according to:

$$\mathbf{C} = \langle \Delta \mathbf{X} \Delta \mathbf{X}^T \rangle \tag{2.9}$$

where $\Delta \mathbf{X} = \mathbf{X}(t) - \langle \mathbf{X} \rangle$ and the angle brackets represent a time or ensemble average. Particles moving in a correlated fashion correspond to positive matrix elements (positive correlation) or negative elements (negative correlation) and those that move independently to small matrix elements. The orthogonal transformation $\mathbf{T}$ that diagonalises this (symmetric) matrix contains the eigenvectors or principal components of $\mathbf{C}$ as columns and the resulting diagonal matrix $\mathbf{\Lambda}$ contains the corresponding eigenvalues:

$$\mathbf{\Lambda} = \mathbf{T}^T \mathbf{C} \mathbf{T} \tag{2.10}$$

The eigenvalues are the positional mean square fluctuations along the corresponding eigenvectors. When the eigenvectors are sorted to decreasing eigenvalues, the first eigenvectors are those collective motions that best approximate the sum of fluctuations and the last eigenvectors correspond to the most constrained degrees of freedom. The characteristics of these collective fluctuations can be studied by

projecting the ensemble of structures onto single eigenvectors and by translation of these projections to 3D space to visualize the atomic displacements connected with that eigenvector. As stated above, analyses of MD trajectories of several proteins have shown that few collective coordinates dominate the dynamics of native proteins (together often referred to as the 'essential subspace'). In a number of cases these main modes of collective fluctuation were shown to be involved in the functional dynamics of the studied proteins.[45, 47, 48]

ED analyses can be applied to any subset of atoms of the ensemble of structures and are not restricted to ensembles generated by MD simulation. Applications to collections of X-ray structures,[48, 49] NMR structures[50] and structures derived from distance constraints[48] have been reported. Since collective (backbone) fluctuations dominate the dynamics of proteins, usually only backbone or Cα coordinates are used to save computation time and to prevent problems with apparent correlation of side chain motions with backbone motions which are merely the result of poor statistics. However, even when the method is applied to only Cα atoms, the diagonalisation of the covariance matrix can still be an enormous computational task.

2.3   Free energy calculations

In general terms, a microscopic description of a particular molecular system can be given in the form of a Hamilton operator or function. This is often simply expressed as the Hamiltonian $H(\boldsymbol{p}, \boldsymbol{q})$ of the generalized coordinates $\boldsymbol{q}$ and their conjugate momenta $\boldsymbol{p}$. For example, the Hamiltonian for a classical system of N atoms, expressed in terms of the Cartesian coordinates $\boldsymbol{r}$ and momenta $\boldsymbol{p}$ of each of the atoms, has the form $H(\boldsymbol{p}, \boldsymbol{r}) = K(\boldsymbol{p}) + U(\boldsymbol{r})$, where K is the kinetic and U the potential energy. In the canonical ensemble the fundamental formula for the Helmholtz free energy, A, is: [51]

$$A(N, V, T) = -k_B T \ln Q(N, V, T) \tag{2.11}$$

where the partition function Q is:

$$Q(N, V, T) = h^{-3N} \int \int e^{-H(\boldsymbol{p}, \boldsymbol{r})/k_B T} d\boldsymbol{p} d\boldsymbol{r} \tag{2.12}$$

where V is the volume of the system, T the absolute temperature, k_B Boltzmann's constant, h Planck's constant, and it is assumed that the N atoms are distinguishable. The factor before the integral actually comes from quantum mechanics. The essential difficulty in calculating the free energy of a system is evident from Eqn. 2.12, which is dipendent on a $6N$-dimensional integral to be carried out over phase space.

By means of statistical mechanics, free energy differences may also be expressed in terms of averages over ensembles of atomic configurations for the molecular system of interest. Such an ensemble can be generated by MC or MD simulation techniques. If the *ergodic hypothesis* is verified, that is the simulated trajectory will visit all possible microstates available to it, given an infinite amount of time the following equivalence holds:

$$\langle \mathcal{A}(\boldsymbol{q}(t), \boldsymbol{p}(t)) \rangle_{ensemble} = \langle \mathcal{A}(\boldsymbol{q}(t), \boldsymbol{p}(t)) \rangle_{time} \qquad (2.13)$$

that is the ensemble average of a generic physical observable, $\mathcal{A}(t)$, is equivalent to its time average. In principle this equivalence offers a valid method, the time average, to obtain physical properties from our "virtual" experiment, namely computer simulations. However, despite its inherent simplicity, the computation of thermodynamic properties from molecular simulations remains far from trivial due to the limit of infinite sampling of phase space and to unavoidable numerical errors.

Within the framework of statistical mechanics, a variety of formulae for determining the difference in free energy between two states of a system, or the projection of such a difference in free energy along a spatial (reaction) coordinate, have been derived. The different formulations available are all equivalent within the limit of infinite sampling of phase space. In practice, as only a part of the total phase space accessible to a realistic system can ever be sampled by molecular simulations techniques, there are often significant differences in accuracy between the free energy estimates obtained from different formulae. Below a list of the most useful statistical mechanical formulae and computational methods to obtain the difference in free energy $\Delta A_{A \to B} = A_B - A_A$ between a state B and a state A of a molecular system in a canonical ensemble is provided.

2.3.1 Probability ratio method

In equilibrium thermodynamics, free energy changes are related to the populations (or probabilities) of states. Hence, the most straightforward way to determine the difference in free energy between two states of a system is simply to count the number of configurations in the two corresponding states. For example, in the case of folding, this involves counting the number of folded conformations N_F and the number of unfolded conformations N_U in an ensemble generated during a MD or MC simulation, with the difference in free energy being given by

$$\Delta A_{U \to F} = -k_B T \ln \frac{Q_F}{Q_U} = -k_B T \ln \frac{p_F}{p_U} = -k_B T \ln \frac{N_F}{N_U} \qquad (2.14)$$

where k_B is the Boltzmann constant, T is the temperature, Q_F and Q_U are the partition functions of the folded and unfolded states, respectively, and p_F and p_U are the probability densities of finding the system in the folded or unfolded states, respectively. This technique is only appropriate when folded and unfolded conformations occur with sufficient frequency in the ensemble to obtain reliable statistics. Direct counting has the advantage that it does not depend on the definition of a reaction coordinate and it is particularly well-suited to situations in which the end states are themselves ensembles of structures, such as in the study of protein/peptide folding.

2.3.2 Thermodynamic Integration

Integrations methods determine the change in free energy between two states of a system from the integral of the work required to go from an initial state to a final state *via* a reversible path. In *Thermodynamic Integration* (TI) method an arbitrary coupling parameter, λ, is introduced in the the Hamiltonian $H(\boldsymbol{p}, \boldsymbol{q}, \lambda)$. The coupling parameter is chosen such that when $\lambda = \lambda_A$ the Hamiltonian of the molecular system corresponds to that of state A, i.e. $H(\boldsymbol{p}, \boldsymbol{q}, \lambda_A) = H(\boldsymbol{p}, \boldsymbol{q})$ and when $\lambda = \lambda_B$ the Hamiltonian of the system corresponds to that of state B, i.e. $H(\boldsymbol{p}, \boldsymbol{q}, \lambda_B) = H(\boldsymbol{p}, \boldsymbol{q})$. If the Hamiltonian is a function of λ the free energy in Eqn. 2.11 will also be a function of λ, and the derivative of the free energy with respect to λ will be given by

$$\frac{dA(\lambda)}{d\lambda} = \left\langle \frac{\partial H(\lambda)}{\partial \lambda} \right\rangle_\lambda \tag{2.15}$$

From this, it follows directly that the free energy difference between state A and state B of a molecular system is given by

$$A(\lambda_B) - A(\lambda_A) = \int_{\lambda_A}^{\lambda_B} \left\langle \frac{\partial H(\lambda)}{\partial \lambda} \right\rangle_\lambda d\lambda \tag{2.16}$$

which is the so-called thermodynamic integration formula.[52] The ensemble average $\langle \partial H / \partial \lambda \rangle$ is most commonly determined from simulations at a series of λ values between λ_A and λ_B and the integral in Eqn. 2.16 evaluated numerically. The choice of λ is arbitrary and λ may equally refer to a spatial coordinate or to a non-physical coordinate in parameter space. In either case, the functional dependence of the system on λ effectively describes the pathway from the initial to the final state.

2.3.3 Perturbation method

An alternative to the TI method is to adopt a perturbation approach. In the *perturbation method* (PM) the free energy change is expressed by the following relation:[53]

$$A_B - A_A = -k_B T \ln \frac{Q_B}{Q_A} = -k_B T \ln \left\langle e^{\Delta H / k_B T} \right\rangle_B \tag{2.17}$$

where Q_B and Q_A are the partition functions of state B and A respectively, $\Delta H = H_B - H_A$ is the energy difference, k_B is the Boltzmann constant and T the absolute temperature. The subscript on the brackets $\langle ... \rangle$ indicates that the ensemble average is performed with respect to the probability function representative of the final state, B, of the system. Thus, the free energy change is calculated directly from one MD simulation of the state B averaging the quantity $e^{\Delta H / k_B T}$. Usually, due to the known insufficient sampling of the tails of the distribution, this method gives accurate results when the energies of the initial and final states of the system differ by a relatively small amount ($\leq 2k_B T$). Otherwise, it is possible to decompose the total free energy change by defining intermediate states along a given path between the initial and final states, hence computing as a sum of partial free energy changes.

2.3.4 Potential of Mean Force

The difference in free energy between two states of a molecular system is a single number. Often we would like to know how the free energy of a system, or the *potential of mean force* (PMF), changes as a function of a particular coordinate within the system, most commonly a spatial coordinate. Chosen this coordinate, r, and considering the partial derivative of the free energy with respect to this coordinate, we obtain:

$$\frac{\partial A}{\partial r} = -k_B T \frac{1}{Q} \frac{\partial Q}{\partial r} = -k_B T \frac{1}{Q} \int \int -\frac{\partial U(\boldsymbol{q})}{\partial r} \frac{1}{k_B T} e^{-H(\boldsymbol{p},\boldsymbol{q})/k_B T} d\boldsymbol{p} d\boldsymbol{q} \qquad (2.18)$$

Considering that $-\partial U(\boldsymbol{q})/\partial r$ is the force acting along r, $\boldsymbol{F}(r)$, and that the average value of a generic function, $f(\boldsymbol{p},\boldsymbol{q})$, is given by:

$$\langle f(\boldsymbol{p},\boldsymbol{q}) \rangle = \frac{1}{Q} \int \int f(\boldsymbol{p},\boldsymbol{q}) e^{-H(\boldsymbol{p},\boldsymbol{q})/k_B T} d\boldsymbol{p} d\boldsymbol{q}, \qquad (2.19)$$

Eqn. 2.18 becomes

$$\frac{\partial A}{\partial r} = -\langle \boldsymbol{F}(r) \rangle \qquad (2.20)$$

Hence, if we are interested in the free energy change between two positions r_A and r_B, we get

$$A_B - A_A = \int_{r_A}^{r_B} -\langle \boldsymbol{F}(r) \rangle dr \qquad (2.21)$$

Usually the ensemble average $-\langle \boldsymbol{F}(r) \rangle$ is most commonly determined from simulations at a series of r values between r_A and r_B and the integral in Eqn. 2.21 evaluated numerically.

THREE

THE QUASI-GAUSSIAN ENTROPY THEORY

3.1 Introduction

Accurate methods to obtain the statistical mechanics and thermodynamics of simulated condensed systems are clearly of great importance as they can provide essential information for describing and predicting the behavior of a molecular complex system. Despite of the great development of the simulation methods, the evaluation of essential thermodynamic properties such as free energy and entropy, and of many related observables, are very difficult and typically the methodologies used can only provide limited "local" information, i.e., a few thermodynamic properties at a given temperature and density, requiring a rather heavy computational effort. Moreover, the basic theoretical principles underlining these methods, i.e., thermodynamic integration (TI) and perturbation method (PM), can be affected by severe problems due to the slow convergence. It is therefore a challenge in theoretical physical chemistry to develope and optimize more analytical methods, based on sound theories, providing the thermodynamics of a simulated system at relatively low computational costs. From a theoretical point of view, the key point is the evaluation of the (configurational) partition function, which is in general a high-dimensional integral over all coordinates. For complex systems with a realistic Hamiltonian, it is virtually impossible to derive in this way rigorous but easy to handle expressions for the various thermodynamic properties. Only for very special Hamiltonians analytical solutions are available, e.g. for the (monoatomic) ideal

gas, a set of quantum or classical harmonic oscillators or one and two-dimensional Ising spin systems. However, in this chapter we will show that it is possible to switch from the description in terms of this high-dimensional partition function in the canonical ensemble to the one-dimensional internal energy distribution function of the system, which is a special projection of the Hamiltonian. The advantage of this approach is the fact that these distributions, because of the macroscopic character of usual systems, are almost Gaussian ("quasi-Gaussian"). Hence mathematically speaking, already relatively simple functions can be used to model the real distributions, yielding very compact expressions for the corresponding thermodynamic functions. The theory based on this, which will be presented in this chapter, will be denoted as the "quasi-Gaussian entropy theory" (QGE).

3.2 The quasi-Gaussian entropy theory in canonical ensemble

In this section the derivation of the basic theory for the temperature dependence of thermodynamics properties in the canonical ensemble is presented. Chosing a proper reference state, the excess entropy S^* can be expressed in terms of the moment generating function of the excess internal energy distribution function $\rho(\Delta \mathcal{U}')$. For a macroscopic system the application of the central limit theorem demonstrates that this distribution function can be modeled as a unimodal function, close to a Gaussian ("quasi-Gaussian"). Hence, from the statistical mechanical definition of $\rho(\Delta \mathcal{U}')$, the generalized Pearson system of distributions can be used to generate and classify unimodal distribution of increasing complexity. The parameters of these distributions and hence of the excess entropy can be expressed in terms of the isochoric heat capacity and a limited set of its temperature derivatives.

3.2.1 Definition of the system

The Helmholtz free energy of a system at fixed volume, temperature and number of molecules is

$$A = -kT \ln Q \tag{3.1}$$

where Q is the overall partition function. For a system of n identical molecules in the classical limit

$$Q = \frac{(2\pi kT)^{d/2}}{n! h^d (1+\gamma)^n} \sum_l \int e^{-\beta(\Phi+\psi+\varepsilon_l)} \prod_{j=1}^{n} (\det \tilde{M}_j)^{1/2} d\mathbf{x} \tag{3.2}$$

where $\mathbf{x}$ are the semiclassical atomic coordinates, Φ is the (classical) intermolecular potential energy, ψ is the (classical) intramolecular potential energy, ε_l is the overall lth quantum energy (in general a function of the coordinates which typically only refers to vibrational states), $\beta = 1/kT$ and the sum runs over all accessible quantum states $\{l\}$ of the system in the temperature range of interest. Moreover d is the total number of semiclassical degrees of freedom of the system, $1 + \gamma$ is the symmetry coefficient of the molecule, h is the Planck constant and $\tilde{M}$ is the (classical) mass tensor of the molecule. We can simplify Eq. 3.2, considering that in general for systems where the (quantum) vibrational energies have a significant dependence on the coordinates, such a dependence is typically observed only up to temperatures where the molecules are largely confined in the vibrational ground state. In such systems, as the temperature is increased to values where the first excited states become significantly populated, the vibrational energies converge to a coordinates independent value, usually close to the ideal gas ones. For these kind of systems we can rewrite Eq.3 as

$$Q \propto \sum_l \int e^{-\beta(\Phi+\psi+\varepsilon_l)} + \prod_{j=1}^{n} (\det \tilde{M}_j)^{1/2} d\mathbf{x} \tag{3.3}$$

$$= \sum_l e^{-\beta E_l} \int e^{-\beta(\Phi+\psi)} e^{-\beta(\varepsilon_l - E_l)} \prod_{j=1}^{n} (\det \tilde{M}_j)^{1/2} d\mathbf{x} \tag{3.4}$$

with E_l a reference quantum energy of the lth state. We assume, at least for all the terms in Eq. 3.4 significantly different from zero (i.e., βE_l not too large), that

$$\int e^{-\beta(\Phi+\psi)} e^{-\beta(\varepsilon_l - E_l)} d\mathbf{x} \prod_{j=1}^{n} (\det \tilde{M}_j)^{1/2} \cong \int e^{-\beta(\Phi+\psi)} e^{-\beta(\varepsilon_0 - E_0)} \prod_{j=1}^{n} (\det \tilde{M}_j)^{1/2} d\mathbf{x}$$

$$\tag{3.5}$$

Hence

$$Q \cong \int e^{-\beta U'} \prod_{j=1}^{n} (\det \tilde{M}_j)^{1/2} d\mathbf{x} \tag{3.6}$$

$$Q_{qm}^{ref} = \sum_l e^{-\beta E_l} \tag{3.7}$$

$$\Theta = \frac{(2\pi kT)^{1/2} Q_{qm}^{ref}}{n! h^d (1+\gamma)^n} \tag{3.8}$$

with $U' = \Phi + \psi + \varepsilon_0 - E_0$ and where E_0 and Q_{qm}^{ref} can be typically obtained by quantum calculations of the isolated molecule, i.e. in ideal gas conditions. It is easy to see that Eq. 3.6 is always exact if the system is completely confined in the vibrational ground state, or if no vibrations are present (e.g. monatomic molecules) or when the vibrational energies can be considered independent of the coordinates, and therefore from the temperature, hence being identical to the ideal gas ones. If moreover, at least in the whole temperature range of interest, only a part of the configurational space is energetically accessible (i.e., the system is confined within a part of the configurational space) we can rewrite Eq. 3.6 as

$$Q \cong Q_{ref}^{qm} \int^* e^{-\beta U'} \prod_{j=1}^{n} (\det \tilde{M}_j)^{1/2} d\mathbf{x} \tag{3.9}$$

where now the star denotes an integration in the accessible part of the configurational space only. It should be noted that the unaccessible configurations not necessarily correspond only to the ones which are forbidden by a simple excluded volume concept, where it is assumed that the pair potential energy has an infinite barrier as in a hard sphere liquid. In fact, according to the *total* intermolecular potential energy, even configurations with non penetrating molecules might be energetically excluded up to very high temperatures. Clearly in the infinite temperature limit every finite energy configuration will be accessible implying that only the confinement due to the infinite energy configurations can be considered exact, i.e., really temperature independent. Eq. 3.9, which reduces to Eq. 3.6 in case the whole configurational space is available, is a very general expression that can be used for many different types of molecules.

3.2.2 Definition of the reference states and excess properties

For all the systems where Eq. 3.9 can be used, we can define a reference state at the same temperature and density, but without inter (Φ) and intramolecular potential energy (ψ). We have

$$
\begin{aligned}
A_{ref} &= -kT \ln Q_{ref} & (3.10)\\
Q_{ref} &= \Theta \int \textstyle\prod_{j=1}^{n} (\det \tilde{M}_j)^{1/2} d\mathbf{x} & (3.11)
\end{aligned}
$$

Therefore the excess Helmholtz free energy is

$$
\begin{aligned}
A' &= A - A_{ref} & (3.12)\\
A' &= A^* - kT \ln \epsilon & (3.13)\\
A^* &= -kT \ln \left\langle e^{-\beta U'} \right\rangle = -kT \ln \left\langle e^{-\beta U'} \right\rangle_{ref} & (3.14)\\
\left\langle e^{\beta U'} \right\rangle &= \frac{\int^* e^{-\beta U'} \prod_{j=1}^{n} (\det \tilde{M}_j)^{1/2} e^{\beta U'} d\mathbf{x}}{\int^* e^{-\beta U'} \prod_{j=1}^{n} (\det \tilde{M}_j)^{1/2} e^{\beta U'} d\mathbf{x}} & (3.15)\\
\left\langle e^{-\beta U'} \right\rangle_{ref} &= \frac{\int^* e^{-\beta U'} \prod_{j=1}^{n} (\delta \tilde{M}_j)^{1/2} d\mathbf{x}}{\int^* \prod_{j=1}^{n} (\det \tilde{M}_j)^{1/2} d\mathbf{x}} & (3.16)\\
\epsilon &= \frac{\int^* \prod_{j=1}^{n} (\det \tilde{M}_j)^{1/2} d\mathbf{x}}{\int \prod_{j=1}^{n} (\det \tilde{M}_j)^{1/2} d\mathbf{x}} & (3.17)
\end{aligned}
$$

Then we can write the internal energy, heat capacity, pressure and entropy as

$$
\begin{aligned}
U' &= -\left(\frac{\partial}{\partial \beta} \ln \frac{Q}{Q_{ref}} \right)_V = \langle U' \rangle & (3.18)\\
C'_V &= \left(\frac{\partial U'}{\partial T} \right)_V = \left(\frac{\partial \langle U' \rangle}{\partial T} \right)_V & (3.19)\\
S' &= -\frac{(A' - U')}{T} = S^* + k \ln \epsilon & (3.20)\\
S^* &= -k \ln \left\langle e^{\beta(U' - \langle U' \rangle)} \right\rangle & (3.21)
\end{aligned}
$$

and

$$p' = -\left(\frac{\partial A'}{\partial V}\right)_T = p^* + T\xi \tag{3.22}$$

$$p^* = -\left(\frac{\partial A^*}{\partial V}\right)_T \tag{3.23}$$

$$\xi = k\left(\frac{\partial ln\epsilon}{\partial V}\right) \tag{3.24}$$

Finally, from these equations follow the excess enthalpy and the Gibbs free energy

$$H' = U' + p'V \tag{3.25}$$

$$G' = A' + p'V \tag{3.26}$$

3.2.3   The potential energy distribution

Eq. 3.21 can be explicitly expressed as

$$S^* = -k \ln G_{\Delta U'}(\beta) = -k \ln \int e^{\beta \Delta U'} \rho(\Delta U') d\Delta U' \tag{3.27}$$

$$\Delta U' = U' - \langle U' \rangle \tag{3.28}$$

where $G_{\Delta U'}(\beta)$ is the moment generating function [54, 55] of the potential energy distribution function $\rho(\Delta U')$ (note that ρ is in general temperature dependent). From the fact that a macroscopic system can be considered as a very large collection of identical, independent subsystems (elementary systems), we can conclude that because of the central limit theorem [54, 56] the corresponding potential energy distribution function can be regarded as uninormal. In fact the possible deviations from the uninormal shape in the far tail of the distribution are in general negligible because of the very sharply peaked behavior of the curve around its mode (maximum of probability), also due to the macroscopic nature of the system [57, 51], and therefore the integrand in Eq. 3.27 can be modeled considering ρ as a quasi-Gaussian distribution. In general we can express the potential energy distribution

as [57, 58]

$$\rho(\Delta U') = \frac{\Omega(\Delta U')}{\int^* e^{-\beta \Delta U'} \prod_{j=1}^{n} (\det \tilde{M}_j)^{1/2} d\mathbf{x}} e^{-\beta \Delta U'} \qquad (3.29)$$

with

$$\Omega(\Delta U') = \int^* \delta(\Delta U'(\mathbf{x}) - \Delta U') \prod_{j=1}^{n} (\det \tilde{M}_j)^{1/2} d\mathbf{x} \qquad (3.30)$$

and hence

$$\frac{d\rho}{d\Delta U'} = -\rho(\Delta U') \left[\beta - \frac{d \ln \Omega}{d\Delta U'} \right] \qquad (3.31)$$

Using a Padé approximant [59, 60], instead of a usual Taylor series, to expand the function between brackets in Eq. 3.31 around the mode of the distribution, we finally obtain a general differential equation, equivalent to the one of the generalized Pearson system of curves [61, 62, 63], which can be used to obtain the possible potential energy distribution functions:

$$\frac{d\rho}{d\Delta U'} = -(\Delta U' - \Delta U'_m)\, \rho\, \frac{P^m(\Delta U')}{G^n(\Delta U')} \qquad (3.32)$$

where $\Delta U'_m$ is the value of $\Delta U'$ where ρ has its mode and $P^m(\Delta U')$ and $G^n(\Delta U')$ are some arbitrary polynomials of order m and n:

$$P^m(\Delta U') \;\; = \;\; \sum_{i=0}^{m} a_i (\Delta U')^i \qquad (3.33)$$

$$G^n(\Delta U') \;\; = \;\; \sum_{j=0}^{n} b_j (\Delta U')^j \qquad (3.34)$$

where without loss of generality $a_0 = 1$. The solutions of Eq. 3.32 are therefore fully defined by the parameters $\Delta U'_m$, $\{a_i\}$ and $\{b_j\}$ which can be expressed [61] in terms of the central potential energy moments M_n. Hence with the use of physical-mathematical restrictions [61] we can select the physically acceptable distributions, fully defined by a limited set of central moments, and then order them according to their increasing complexity. We also showed that these potential energy moments

can be expressed as a function of the isochoric heat capacity and a limited number of its temperature derivatives [61]

$$M_2(T) = kT^2 C_V'$$ (3.35)

$$M_3(T) = (kT^2)^2 \left(\frac{\partial C_V'}{\partial T}\right)_V + 2(kT)^2 T C_V'$$ (3.36)

$$\cdots$$

$$M_k(T) = M_k\left(T, C_V', \left(\frac{\partial C_V'}{\partial T}\right)_V, \left(\frac{\partial^2 C_V'}{\partial T^2}\right)_V, \cdots, \left(\frac{\partial^{k-2} C_V'}{\partial T^{k-2}}\right)_V\right)$$ (3.37)

where $M_k = \langle (\Delta U')^k \rangle$ is the kth central potential energy moment and we used the fact that $C_V^* = C_V'$. If the functional shape of ρ is defined by the first n central moments, from Eqs. 3.27 and 3.37 it follows that

$$S^* = S^*\left(T, C_V', \left(\frac{\partial C_V'}{\partial T}\right)_V, \left(\frac{\partial^2 C_V'}{\partial T^2}\right)_V, \cdots, \left(\frac{\partial^{n-2} C_V'}{\partial T^{n-2}}\right)_V\right)$$ (3.38)

3.2.4 The thermodynamic master equation

We define the *intrinsic entropy function* as [61]

$$\alpha = \frac{S'}{C_V'} = \frac{S^*}{C_V'} + \frac{k \ln \epsilon}{C_V'}$$

$$= \alpha^*\left(T, C_V', \left(\frac{\partial C_V'}{\partial T}\right)_V, \left(\frac{\partial^2 C_V'}{\partial T^2}\right)_V, \cdots, \left(\frac{\partial^{n-2} C_V'}{\partial T^{n-2}}\right)_V\right) + \frac{k \ln \epsilon}{C_V'} \quad (3.39)$$

with $\alpha^* = S^*/C_V'$ the *confined* intrinsic entropy function, and using the general thermodynamic relation $(\partial S'/\partial T)_V = (\partial S^*/\partial T)_V = C_V'/T$, we obtain the *thermodynamic master equation* [61] (TME)

$$\frac{C_V'}{T} = C_V'\left(\frac{\partial \alpha^*}{\partial T}\right)_V + \alpha^*\left(\frac{\partial C_V'}{\partial T}\right)_V$$ (3.40)

This is a completely defined differential equation where its unique, always existing solution gives the temperature dependence of the ideal reduced isochoric heat capacity C_V', once the values of $C_V', \cdots, (\partial^{n-2} C_V')/(\partial T^{n-2}))_V$ at one arbitrary temperature T_0 are known. Note that in Eqs. 3.39 and 3.40 we used a generalized

expression of the intrinsic entropy function, treating explicitly the possible confinement of the system, which reduces to the usual one when $\epsilon = 1$ and therefore $\alpha = \alpha^*$. From the solution of the master equation we can obtain the confined entropy S^* via Eq. 3.38, and then the excess internal energy and free energy at fixed density via

$$
\begin{aligned}
U'(T) &= U'(T_0) + \int_{T_0}^{T} C_V'(T)dT & (3.41) \\
A^*(T) &= U'(T) - TS^*(T) & (3.42)
\end{aligned}
$$

It is interesting to note that, since

$$
\alpha^* = \frac{S^*}{C_V'} = -\frac{S^*/\beta}{(\partial S^*/\partial\beta)_V} \tag{3.43}
$$

the confined intrinsic entropy function is the ratio between the average slope of S^* versus β (remembering that $S^* = 0$ when $\beta = 0$) and the instantaneous slope $(\partial S^*/\partial\beta)_V$. One can moreover prove that [61, 64]

$$
\lim_{T\to\infty} \alpha^*(T) = -\frac{1}{2} \tag{3.44}
$$

which implies that the (confined) thermodynamics of every system in the infinite temperature limit tends to a Gaussian one, see section 3.3.1.

3.2.5   The conjugated pressure equation

From Eq. 3.38 it is moreover possible to obtain the excess pressure of the system p' as a function of the temperature. In fact from the basic thermodynamic relation

$$
\left(\frac{\partial S^*}{\partial V}\right)_T = \left(\frac{\partial p^*}{\partial T}\right)_V \tag{3.45}
$$

we obtain

$$
\frac{1}{T}\left(\frac{\partial C_V'}{\partial V}\right)_T = \left(\frac{\partial^2 p^*}{\partial T^2}\right)_V \tag{3.46}
$$

and hence in general

$$\left(\frac{\partial f_0}{\partial V}\right)_T = T\left(\frac{\partial^2 p^*}{\partial T^2}\right)_V \tag{3.47}$$

$$\left(\frac{\partial f_1}{\partial V}\right)_T = \left(\frac{\partial^2 p^*}{\partial T^2}\right)_V + T\left(\frac{\partial^3 p^*}{\partial T^3}\right)_V \tag{3.48}$$

$$\cdots \tag{3.49}$$

$$\left(\frac{\partial f_l}{\partial V}\right)_T = l\left(\frac{\partial^l+1 p^*}{\partial T^l+1}\right)_T + T\left(\frac{\partial^l+2 p^*}{\partial T^l+2}\right)_V \tag{3.50}$$

where

$$f_0 = C_V' \; ; \qquad f_1 = \left(\frac{\partial C_V'}{\partial T}\right)_V \; ; \qquad f_l = \left(\frac{\partial^l C_V'}{\partial T^l}\right)_V \tag{3.51}$$

Therefore from Eqs. 3.38, 3.39 and 3.45 we finally obtain another closed differential equation at fixed density for the temperature dependence of the confined pressure p^*, the *conjugated pressure equation* (CPE)

$$\left(\frac{\partial p^*}{\partial T}\right)_V = T\alpha^*(T)\left(\frac{\partial^2 p^*}{\partial T^2}\right)_V + C_V'\left(\frac{\partial \alpha^*}{\partial V}\right)_T \tag{3.52}$$

or, equivalently, using Eqs. 3.38 and 3.46-3.51

$$\begin{aligned}
\left(\frac{\partial p^*}{\partial T}\right)_V &= \sum_l \left[\left(\frac{\partial S^*}{\partial f_l}\right)_{T,f_l}, \left(\frac{\partial f_l}{\partial V}\right)_T\right] \\
&= \sum_l \left[\left(\frac{\partial S^*}{\partial f_l}\right)_{T,f_l}, \left\{l\left(\frac{\partial^{l+1} p^*}{\partial T^{l+1}}\right)_V + T\left(\frac{\partial^{l+2} p^*}{\partial T^{l+2}}\right)_V\right\}\right]
\end{aligned} \tag{3.53}$$

with $l' \neq l$ and $l = 0, \cdots, (n-2)$. Eq. 3.52 or 3.53 can be solved once the first $n-1$ temperature derivatives of the confined pressure are known at one arbitrary temperature T_0. Its solution provides the temperature dependence of $(\partial p^*/\partial T)_V$ for a system at fixed density and, if the excess pressure is known at one temperature as well, also the temperature dependence of the excess pressure, enthalpy and Gibbs free energy via

$$p'(T) = p'(T_0) + \int_{T_0}^{T} \left(\frac{\partial p^*}{\partial T}\right)_V dT + \xi(T - T_0) \tag{3.54}$$

$$H'(T) = U'(T) + p'(T)V \tag{3.55}$$

$$G'(T) = A'(T) + p'(T)V \tag{3.56}$$

Note that it is not necessary to explicitly solve the conjugated pressure differential equation if the temperature dependence of A^* is already known from the thermodynamic master equation, since $p^*(T) = -(\partial A^*(T)/\partial V)_T$. As $A^*(T)$ is an explicit function of T only, with U_0', C_{V0}', $(\partial C_{V0}'/\partial T)_V$, $\cdots$ as parameters (i.e., the values of U' etc. at the reference temperature T_0) depending only on the volume, the resulting volume derivatives at T_0 can be related to p_0^*, $(\partial p_0^*/\partial T)_V$, $(\partial^2 p_0^*/\partial T^2)_V$, $\cdots$, according to Eqs. 3.47-3.51 (see also the description of the Gamma and Inverse Gaussian states).

Hence the knowledge of the potential energy distribution function at one temperature, as well as the knowledge of ϵ and ξ fully defines the whole excess thermodynamics of a system at every temperature at fixed density. Every potential energy distribution function therefore defines a different statistical state of the system with a thermodynamical complexity given by the number of the heat capacity temperature derivatives, necessary to define the corresponding type of potential energy distribution function.

3.2.6 Phase-space confinement

A very simple model for the phase-space confinement as introduced in Eq. **??** is excluded volume due to "hard body" interactions. If, because of the strong Pauli repulsions at close contact, it is possible to define for (almost) spherical molecules like water an interparticle distance $\sigma_{HS} = 2r_{HS}$ at which the two-particle interaction energy is virtually infinite in the temperature range of interest, the confined ideal reference state can be described as a hard sphere (HS) system [51, 65]. Using the Carnahan-Starling equation of state (EOS) [66],

$$p_{HS} = \rho_N kT \left[\frac{1 + \eta + \eta^2 - \eta^3}{(1 - \eta)^3}\right] \tag{3.57}$$

with p_{HS} the pressure, $\eta = v\rho_N$, ρ_N the number density, $v = \pi\sigma_{HS}^3/6$ the hard-sphere volume per molecule and σ_{HS} the hard-sphere diameter, we obtain [65] for the excess Helmholtz free energy, Eq. **??**

$$A'_{ref} = -NkT \left[\frac{3\eta^2 - 4\eta}{(1-\eta)^2} \right] = -NkT \ln \bar{\epsilon}_{HS} \tag{3.58}$$

where $\bar{\epsilon}_{HS} = \epsilon_{HS}^{1/N}$ is the hard sphere phase-space fraction *per molecule*. Hence

$$\bar{\epsilon}_{HS} = \exp \left\{ \frac{3\eta^2 - 4\eta}{(1-\eta)^2} \right\} \tag{3.59}$$

and

$$\xi_{HS} = Nk \frac{d\ln \bar{\epsilon}_{HS}}{dV} = -\frac{Nk}{V} \left[\frac{2\eta^2 - 4\eta}{(1-\eta)^3} \right] \tag{3.60}$$

which is always positive since $\eta < 1$. Within this model, p^* is the pressure of the system with respect to a HS fluid at the same temperature and density. For more complex molecules deviating from an almost spherical shape a simple HS description may not be sufficient. For non spherical molecules several equation of state have been proposed.

3.3   Description of different statistical states

In this section the temperature dependence of thermodynamic properties for different statistical states are presented. In particular, the simplest solutions of the Generalized Pearson systems, the Gaussian and Gamma states, are discussed in details.

3.3.1   Gaussian state

The symmetric Gaussian distribution corresponds to $\{m = 0, n = 0\}$ in the generalized Pearson system, Eq. 3.32. The distribution is given by

$$\rho(\Delta U') = \frac{1}{\sqrt{2\pi b_0}} \exp \left\{ -\frac{\Delta U'^2}{2b_0} \right\} \tag{3.61}$$

with $b_0 = M_2$. Using the fact that the moment generating function of a Gaussian is simply [61, 54, 67]

$$G_{\Delta U'}(\beta) = \exp\left\{\frac{b_0 \beta^2}{2}\right\} \tag{3.62}$$

and expressing M_2 in terms of C_V' (Eq. 3.35), we obtain for the confined intrinsic entropy function

$$\alpha^* = -\frac{1}{2} \tag{3.63}$$

The thermodynamic master equation (TME), Eq. 3.40, therefore reduces to

$$\left(\frac{\partial C_V'}{\partial T}\right)_V = -2\frac{C_V'}{T} \tag{3.64}$$

the solution of which provides for a confined Gaussian state [61]

$$\alpha^*(T) = -\frac{1}{2} \tag{3.65}$$

$$C_V'(T) = C_{V0}'\left(\frac{T_0}{T}\right)^2 \tag{3.66}$$

$$S'(T) = -\frac{1}{2}C_{V0}'\left(\frac{T_0}{T}\right)^2 + k\ln\epsilon \tag{3.67}$$

$$U'(T) = U_0' + T_0 C_{V0}'\left(1 - \frac{T_0}{T}\right) \tag{3.68}$$

and

$$A'(T) = U_0' + T_0 C_{V0}'\left(1 - \frac{T_0}{2T}\right) - kT\ln\epsilon \tag{3.69}$$

where U_0' and C_{V0}' are the values of U' and C_V' at an arbitrary reference temperature T_0. Since $(\partial\alpha^*/\partial V)_T = 0$, the conjugated pressure equation (CPE), Eq. 3.52 is in this case a simple first order differential equation

$$\left(\frac{\partial p^*}{\partial T}\right)_V = -\frac{1}{2}T\left(\frac{\partial^2 p^*}{\partial T^2}\right)_V \tag{3.70}$$

The solution is

$$p^*(T) = p_0^* + T_0 \left(\frac{\partial p_0^*}{\partial T}\right)_V \left(1 - \frac{T_0}{T}\right) \tag{3.71}$$

where p_0^* and $(\partial p_0^*/\partial T)_V$ are the values at the reference temperature T_0. The excess pressure $p'(T)$ follows from Eq. 3.71, using $p' = p^* + T\xi$ and $(\partial p'/\partial T)_V = (\partial p^*/\partial T)_V + \xi$ (Eq. 3.22):

$$p'(T) = p_0' + T_0 \left\{ \left(\frac{\partial p_0'}{\partial T}\right)_V - \xi \right\} \left(1 - \frac{T_0}{T}\right) + \xi(T - T_0) \tag{3.72}$$

It must be noted that only for the confined properties the infinite temperature limits are always physically meaningful.

3.3.2   Gamma state

The Gamma distribution, given by [61, 64, 54]

$$\rho(\Delta U') = \frac{b_1 (1/b_1^2)^{b_0/b_1^2}}{\Gamma(b_0/b_1^2)} \left(b_0 + b_1 \Delta U'\right)^{b_0/b_1^2 - 1} \exp\left\{-\frac{b_0 + b_1 \Delta U'}{b_1^2}\right\} \tag{3.73}$$

with $\Gamma(\cdot)$ the Gamma function [?], $b_0 = M_2$ and $b_1 = M_3/(2M_2)$, corresponds to the $\{m = 0, n = 1\}$ solution of the generalized Pearson system, Eq. 3.32.

The moment generating function of this Gamma distribution is [61, 54, 67]

$$G_{\Delta U'}(\beta) = \exp\left\{-\beta \frac{b_0}{b_1}\right\} (1 - \beta b_1)^{-b_0/b_1^2} \tag{3.74}$$

and expressing the central moments M_2 and M_3, appearing in b_0 and b_1, in terms of C_V' and $(\partial C_V'/\partial T)_V$ (Eqs. 3.35-3.36), the confined intrinsic entropy function is in this case given by [61]

$$\alpha^* = \frac{1}{\delta} + \frac{1}{\delta^2} \ln(1 - \delta) \tag{3.75}$$

with

$$\delta = \frac{M_3}{2kTM_2} = \frac{T \left(\partial C_V'/\partial T\right)_V}{2C_V'} + 1 \tag{3.76}$$

The expression of α^*, combined with the general thermodynamic master equation
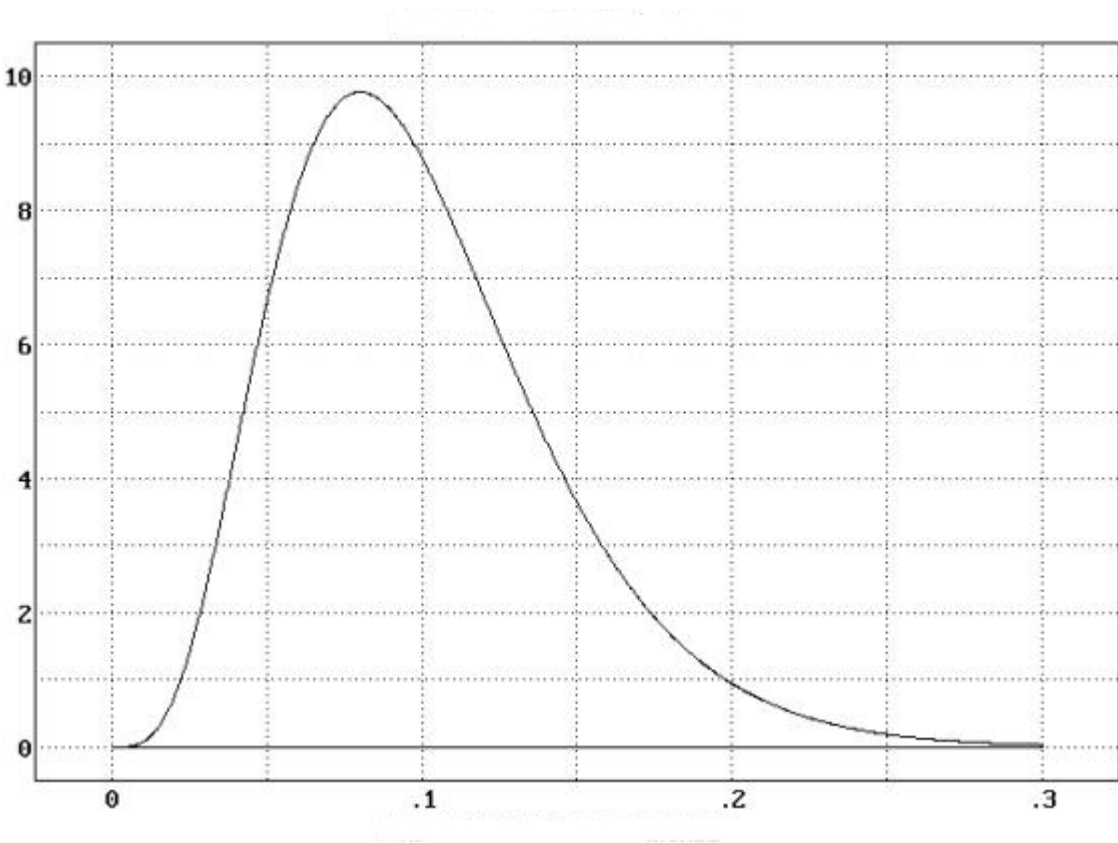
Figure 3.1: The Gamma distribution

(Eq. 3.40), yields

$$T \left(\frac{\partial \alpha^*}{\partial T} \right)_V + 2(\delta - 1)\alpha^* - 1 = 0 \tag{3.77}$$

where $(\partial \alpha^*/\partial T)_V = (d\alpha^*/d\delta)\,(\partial \delta/\partial T)_V$ and $(d\alpha^*/d\delta)$ follows from Eq. 3.75. After straightforward algebra we obtain as a simple form of the TME

$$\left(\frac{\partial \delta}{\partial T} \right)_V = -\frac{\delta(1 - \delta)}{T} \tag{3.78}$$

The solution provides $\delta(T)$, which can be expressed in terms of C'_V and $(\partial C'_V/\partial T)_V$. Hence this gives rise to a new differential equation in C'_V, the solution of which yields for a confined Gamma state [61, 64]

$$\delta(T) = \frac{T_0 \delta_0}{T(1 - \delta_0) + T_0 \delta_0} \tag{3.79}$$

$$\alpha^*(T) = \frac{1}{\delta(T)} + \frac{1}{\delta^2(T)} \ln\{1 - \delta(T)\} \tag{3.80}$$

$$C'_V(T) = C'_{V0} \left(\frac{\delta(T)}{\delta_0} \right)^2 \tag{3.81}$$

$$S'(T) = \frac{C'_{V0}}{\delta_0^2} \left[\delta(T) + \ln\{1 - \delta(T)\} \right] + k \ln \epsilon \tag{3.82}$$

$$U'(T) = U'_0 + (T - T_0)\,C'_{V0}\,\frac{\delta(T)}{\delta_0} \tag{3.83}$$

$$A'(T) = U'_0 - \frac{T_0 C'_{V0}}{\delta_0} - \frac{T C'_{V0}}{\delta_0^2} \ln\{1 - \delta(T)\} - kT \ln \epsilon \tag{3.84}$$

with δ_0 the value of δ at T_0. Note that $(\partial C'_V/\partial T)_V$ is always negative, like in the Gaussian state. Since for a Gamma state the pressure differential equation (Eq. 3.52) is very complicated, it is more convenient to obtain the $p*$ via the volume derivative of $A^*(T)$, using Eq. 3.84. Thus, with the usual notation where $(\partial U'_0/\partial V)_T$ etc. are the derivatives evaluated at T_0

$$p^*(T) = - \left[\frac{\partial A^*}{\partial U'_0} \left(\frac{\partial U'_0}{\partial V} \right)_T + \frac{\partial A^*}{\partial C'_{V0}} \left(\frac{\partial C'_{V0}}{\partial V} \right)_T + \frac{\partial A^*}{\partial \delta_0} \left(\frac{\partial \delta_0}{\partial V} \right)_T \right] \tag{3.85}$$

where from general thermodynamic relations we have

$$\left(\frac{\partial U_0'}{\partial V}\right)_T = T_0 \left(\frac{\partial p_0^*}{\partial T}\right)_V - p_0^* \tag{3.86}$$

$$\left(\frac{\partial C_{V0}'}{\partial V}\right)_T = T_0 \left(\frac{\partial^2 p_0^*}{\partial T^2}\right)_V \tag{3.87}$$

and

$$\left(\frac{\partial \delta_0}{\partial V}\right)_T = \frac{1}{C_{V0}'} \left(\frac{d\alpha_0^*}{d\delta_0}\right)^{-1} \left[\left(\frac{\partial p_0^*}{\partial T}\right)_V - \alpha_0^* T_0 \left(\frac{\partial^2 p_0^*}{\partial T^2}\right)_V\right] \tag{3.88}$$

as follows from the CPE at T_0, with $(d\alpha_0^*/d\delta_0)$ following from Eq. 3.75. The derivatives $\partial A^*/\partial U_0'$, $\partial A^*/\partial C_{V0}'$ and $\partial A^*/\partial \delta_0$ follow from Eq. 3.84. After tedious but straightforward algebra we finally obtain

$$p^*(T) = p_0^* + B_0^* + B_1^* \frac{T}{T(1-\delta_0) + T_0\delta_0} + B_2^* \frac{T}{T_0} \ln\left\{\frac{T(1-\delta_0)}{T(1-\delta_0) + T_0\delta_0}\right\} \tag{3.89}$$

where

$$B_i^* = A_{i1} T_0 \left(\frac{\partial p_0^*}{\partial T}\right)_V + A_{i2} T_0^2 \left(\frac{\partial^2 p_0^*}{\partial T^2}\right)_V \quad i = 0, 1, 2 \tag{3.90}$$

with

$$2A_{01} = -\frac{2(1-\delta_0)\ln(1-\delta_0) + \delta_0}{D} \tag{3.91}$$

$$A_{02} = \frac{1}{\delta_0} \frac{(1-\delta_0)\ln(1-\delta_0) + \delta_0}{D}$$

$$A_{11} = \frac{\delta_0}{D} \tag{3.92}$$

$$A_{12} = -\frac{1}{\delta_0} \frac{\ln(1-\delta_0) + \delta_0}{D} \tag{3.93}$$

$$A_{21} = \frac{2(1-\delta_0)}{D} \tag{3.94}$$

$$A_{22} = \frac{1}{D}$$

and

$$D = 2(1-\delta_0)\ln(1-\delta_0) + \delta_0(2-\delta_0) \tag{3.95}$$

The excess pressure $p'(T)$ follows from Eq. 3.89, using $p' = p^* + T\xi$, $(\partial p'/\partial T)_V =$

$(\partial p^*/\partial T)_V + \xi$ and $(\partial^2 p'/\partial T^2)_V = (\partial^2 p^*/\partial T^2)_V$ (Eq. 3.22):

$$p'(T) = p'_0 + B_0 + B_1 \frac{T}{T(1-\delta_0) + T_0\delta_0} + B_2 \left(\frac{T}{T_0}\right) \ln\left\{\frac{T(1-\delta_0)}{T(1-\delta_0) + T_0\delta_0}\right\} + \xi T$$

(3.96)

where

$$B_0 = A_{01}T_0 \left(\frac{\partial p'_0}{\partial T}\right)_V + A_{02}T_0^2 \left(\frac{\partial^2 p'_0}{\partial T^2}\right)_V + A_{03}T_0\xi \qquad (3.97)$$

$$B_i = A_{i1}T_0 \left\{\left(\frac{\partial p'_0}{\partial T}\right)_V - \xi\right\} + A_{i2}T_0^2 \left(\frac{\partial^2 p'_0}{\partial T^2}\right)_V \quad i = 1, 2 \qquad (3.98)$$

and

$$A_{03} = -\frac{\delta_0(1-\delta_0)}{D} \qquad (3.99)$$

As pointed out previously [64], since the Gamma distribution has a limited domain, it can be defined either from $-\infty$ to some upper limit or from some under limit to $+\infty$. The first case corresponds to a distribution with an asymmetric tail on the left (defining the negative Gamma state Γ_-, with $\delta < 0$ and $-\frac{1}{2} < \alpha^* < 0$), the second case corresponds to an asymmetric tail on the right (defining the positive Gamma state Γ_+, with $0 < \delta < 1$ and $\alpha^* < -\frac{1}{2}$). Note that for $\delta = 0$ the distribution is a Gaussian. The properties of and differences between the two Gamma states have been described in detail [64].

Basically, the Γ_+ state is physically acceptable in the whole semi-classical temperature range, whereas the Γ_- state must be considered as an approximation to a more complicated statistical state within some temperature interval. Because of the finite upper energy limit in a Γ_- distribution, the approximation will be worse for increasing temperature. One other difference is the low temperature limit: while a Γ_+ state may be extrapolated to $T \to 0$ (although of course in that limit the semi-classical description is not valid any more), for a Γ_- state there exist a temperature

$$T_* = -T_0\delta_0/(1-\delta_0) > 0 \qquad (3.100)$$

at which the solution encounters a singularity.

THEORETICAL AND COMPUTATIONAL CHARACTERIZATION OF THE THERMODYNAMIC EFFECTS OF EXTERNAL ELECTRIC FIELDS IN DILUTE IONIC SOLUTIONS

Summary

In this chapter we use the quasi-Gaussian entropy theory in combination with molecular dynamics simulations to provide a detailed description of the thermodynamic variations due to an external electric field. Results show that water polarization as induced by the external (homogenous) electric field, while essentially providing a simple mean energy shift in pure liquid water, determines a complex response in ionic solutions involving entropic variations as a consequence of the competing ion and external fields.

4.1 Introduction

Characterization of liquids and solutions under the effect of external (static) electric fields is a long standing and challenging field of investigation for both theoretical and experimental physical chemistry. In particular, the thermodynamic and kinetic variations induced by the applied electric may be of extreme interest, not only to understand the response of a complex system like a liquid exposed to an external field, but also to obtain essential informations for designing nanotechnological devices for chemical industry.

In the last decade indeed an increasing number of papers [68, 9, 12, 11, 10, 14, 15] has been devoted to such type of research, providing many relevant data mostly concerning structural properties. However, almost no investigation on the thermodynamic response to an external electric field is available in literature, although the thermodynamic variations due to an applied field may be of great importance in fundamental as well as applied research. In a previous paper [69], combining molecular dynamics simulations and the quasi-Gaussian entropy (QGE) theory (essentially an extension of statistical mechanical fluctuation theory) we quantitatively characterized the thermodynamics of liquid water, including its dieletric properties, as a function of temperature and external electric field intensity.

In this paper, following our previous articles [70, 71, 72] we construct a theoretical-computational detailed model for the thermodynamics of ionic solutions (i.e. aqueous sodium and chloride ion solutions at ionic infinite dilution) in the presence of an external static electric field of increasing intensity, characterizing its thermodynamic effects on the ion partial molar properties.

4.2 Theory and Computational Methods

In the quasi-Gaussian entropy (QGE) theory [61, 73, 74, 75] the fundamental expressions of statistical mechanics are rewritten in terms of the distribution function of the fluctuations of a macroscopic propery, as the potential energy (excess energy), expressing the thermodynamics of the system, including the partial molar properties in solutions [70, 71], via analytical models fully defined by the fluctuations distribution.

In a previous paper [69] we characterized the thermodynamic effect, in particu-

lar the dieletric response, due to the presence of increasing external electric fields, clearly showing that the use of the gamma-state level of the QGE theory is accurate.

Similar models, based on the combination of the QGE theory with Molecular Dynamics (MD) simulations, have been also used to provide an accurate description of the thermodynamics of many solutes at infinite dilutions [70, 71] in usual thermodynamic conditions (i.e. no applied external fields). In a recent paper [72] we extended the QGE method to treat conformational transitions in solvated molecules (multi-Gamma-state model) by defining different states along a given set of conformational coordinates. Such a procedure may be utilized not only for conformational transitions, but in principle for any state transition as defined by a set of parameters of the system's Hamiltonian. Therefore, following our previous paper [72], we may express the chemical potential change due to the external (homogenous) electric field (with respect to the zero field state) at isochoric condition (i.e. the system's volume is constant) via

$$\Delta\mu(T, E_0) = \Delta u_0^{'} - \Delta c_{V0}^{'} T_0 \Delta(T) + \Delta[p^{'}(T)v] - RT \ln \gamma \qquad (4.1)$$

where $\Delta u_0^{'}$ and $\Delta c_{V0}^{'}$ are the partial molar excess internal energy and isochoric heat capacity shifts as obtained at the reference temperature T_0, hence depending only on the external electric field E_0, $p^{'}$ is the excess pressure of the system, v is the partial molar volume that within the model used is temperature independent [70, 71, 72] and therefore a function of the external field only, γ is a temperature independent factor essentially given by the ratio of the fractions of accessible phase space [72] and

$$\Lambda(T) = \frac{1}{\delta_0} + \frac{T}{T_0 \delta_0^2} \ln \left[\frac{T(1 - \delta_0)}{T(1 - \delta_0) + T_0 \delta_0} \right] \qquad (4.2)$$

with δ_0 a dimensionless constant.

Note that within solute infinite dilutions conditions, $p^{'}$ and Λ, being intensive properties, are fully determined by the solvent, that is they are identical to the corresponding pure solvent (Gamma state) properties [70, 71, 73]. Moreover, in a homogeneous liquid both δ_0 and the fraction of accessible phase space may be considered as field independent [69], and hence for pure water $\gamma \simeq 1$, $\Delta v = 0$ (isochoric conditions) and for an infinitely diluted solute δ_0 is given by the zero

field pure water system (note that, in general, for the solute condition $\gamma \neq 1$). According to the previous equations and following again our previous paper [72] we may also express the partial molar entropy and internal energy shifts by

$$\Delta s(T, E_0) = \frac{T_0 \Delta c'_{V0}}{T} \left[\frac{T - T_0}{T(1 - \delta_0) + T_0 \delta_0} + \Lambda(T) \right] + R \ln \gamma + \rho_s R \Delta v \qquad (4.3)$$

$$\Delta u(T, E_0) = \Delta u'_0 + \left[\frac{(T - T_0) T_0 \Delta c'_{V0}}{T(1 - \delta_0) + T_0 \delta_0} \right] \qquad (4.4)$$

with ρ_s the solvent molar density.

In order to parametrize the QGE model outlined above, we followed the procedure described in our previous paper [72] utilizing three sets of (isochoric) molecular dynamics (MD) simulations in the 280–1000 K temperature range: for the first set of simulations we used a cubic box of 256 simple point charge (SPC) [76] water molecules, at 55.32 mol/l; in the other sets of simulations we used the same SPC system adding a single sodium or chloride ion kept fixed at the centre of the box (note that for solute infinite dilution the solute-solvent thermodynamics can be obtained considering a single solute molecule embedded in a large amount of solvent molecules). Note that the use of the SPC to describe liquid water instead of the more recent SPC/E model [77], improving the reproduction of the self diffusion coefficient, radial distribution and dielectric constant, is motivated by the worst accuracy of SPC/E with to respect SPC in reproducing liquid water partial molar thermodynamic properties such as the chemical potential, the entropy etc [70, 78, 79]. All the simulations were performed using the GROMACS [80, 81] software package modified to use the isokinetic temperature coupling [82]. For all the simulations the number of steps was 3000000 with three different time steps: 2 fs for simulations in the temperature range 280–370 K, 1 femtosecond in the temperature range 420–800 K and 0.5 fs at $T = 1000$ K, respectively. Hence the corresponding simulation temporal lengths are about 6, 3 and 1.5 ns. Short range interactions were evaluated within 0.9 nm cut off radius and the long range electrostatics was calculated using the Particle Mesh Ewald (PME) method [83]. It is worth to note that within our simulation procedure the interaction between the ion and its replica is removed, and hence the simulation box defined by 256 water molecules and a

single ion provides a good description of high dilution condition [70]. Each set of simulations contains MD trajectories performed at 8 different temperatures and using 4 external electric fields conditions (0 1 3 5 V/nm). Note that for the present case we obtained from the MD simulations the chemical potential variations to be used in the QGE model parameterization via:

$$\Delta\mu(T, E_0) = \int_0^{E_0} [M(T, E_0') - M_w(T, E_0')]dE_0' \qquad (4.5)$$

With M, M_w the mean electric moment along the external field direction for the solute-solvent and pure solvent system respectively. In addition, we also performed other MD simulations at 300 K, utilizing electric field intensities in the range 0.04–5 V/nm.

4.3 Results and discussions

As evidenced in our previous paper [69], the main effect due to a homogenous external field of increasing intensity for liquid water, as obtained by the QGE model based on MD simulations, consists in an almost temperature independent linear shift of the chemical potential (see figure 4.1), implying that the increasing water polarization has little effect on the system's entropy.

In figure 4.2 it is shown the same effect for the water molar excess energy (essentially the mean potential energy), indeed indicating an almost temperature independent polarization effect. Note that in the figure we compare the molar excess energy as obtained by MD data with the curves provided by the QGE models, clearly illustrating the accuracy of the Gamma-state level of the theory in quantitatively describing the liquid behavior.

In figures 4.3 and 4.4 we report the chemical potential variation due to the field intensity as provided by the QGE models for solvated sodium and chloride ions at infinite dilution. From the figures it is evident that now water polarization effects provide a more complex response with a clear temperature dependence of the chemical potential change, hence indicating a significant field and temperature dependence of the ion partial molar internal energy and entropy (see figures 4.5-4.8).

It is worth to note that for both ions a clear transition in thermodynamic
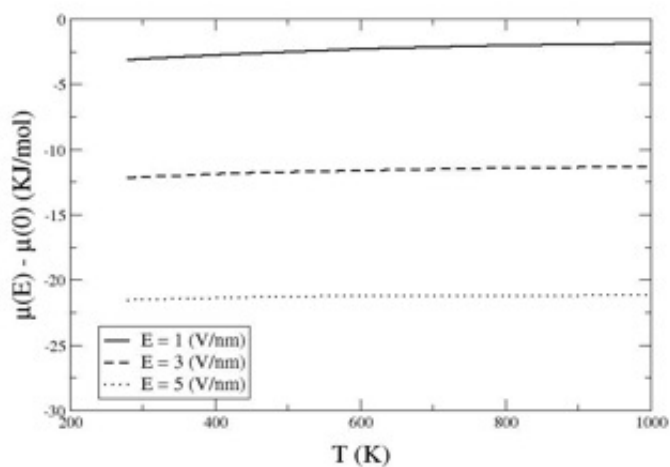
Figure 4.1: **The excess chemical potential shift of pure SPC water with respect to the reference state (without the electric field).**
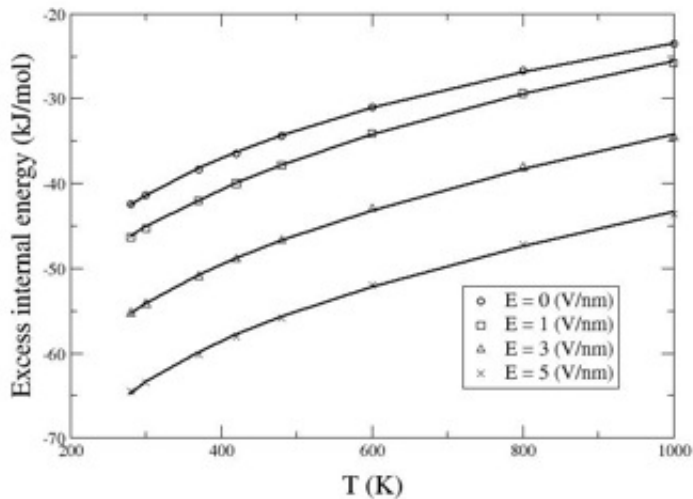
Figure 4.2: **Comparison of the molar excess internal energy of pure SPC water as obtained by the QGE model (solid lines) and MD data (symbols) for different electric field intensities.**
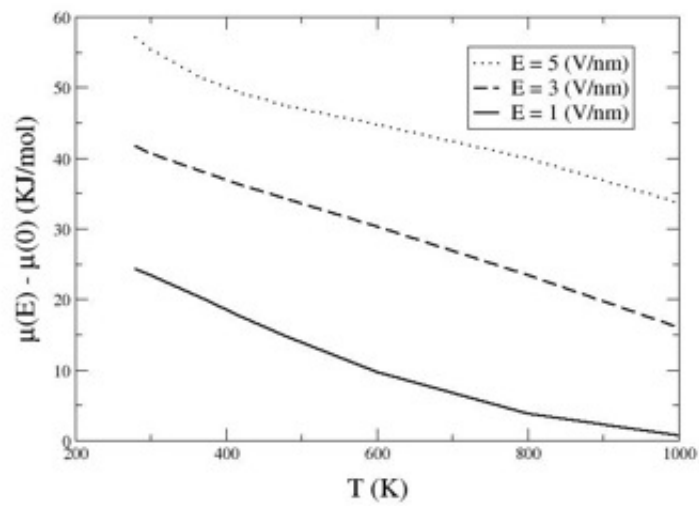
Figure 4.3: **Excess chemical potential shift of sodium ion.**
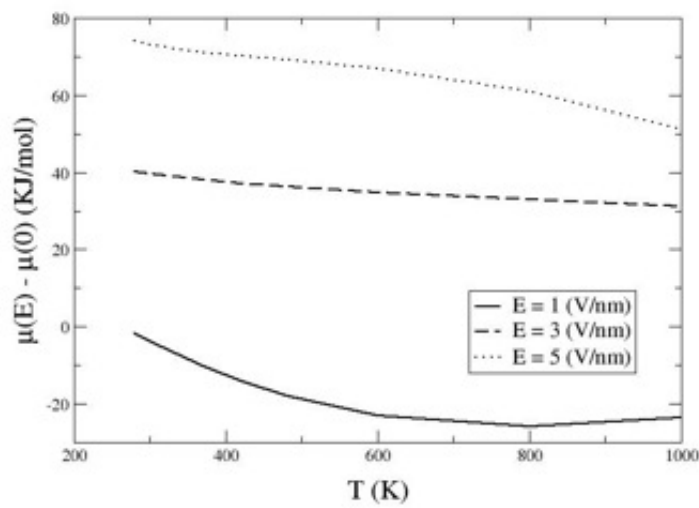
Figure 4.4: **Excess chemical potential shift of chloride ion.**
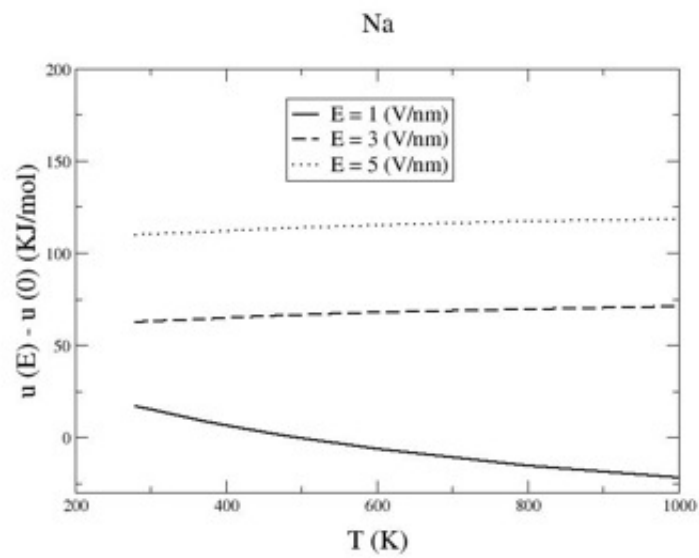
Figure 4.5: **Partial molar energy shift of sodium ion.**
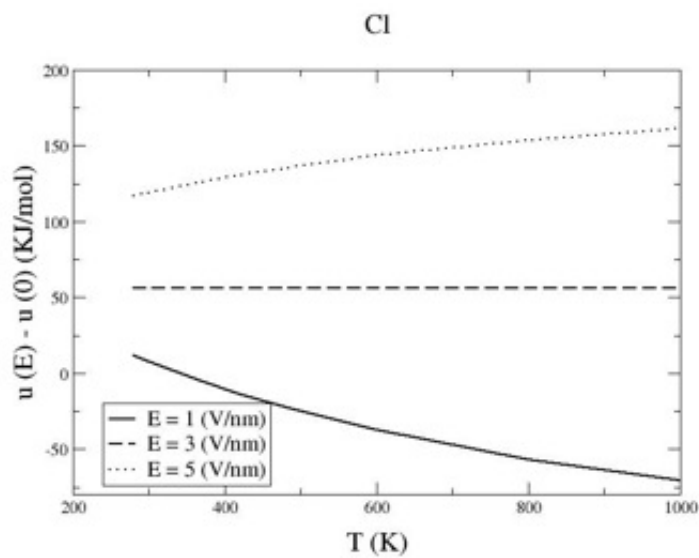
Figure 4.6: **Partial molar energy shift of chloride ion.**
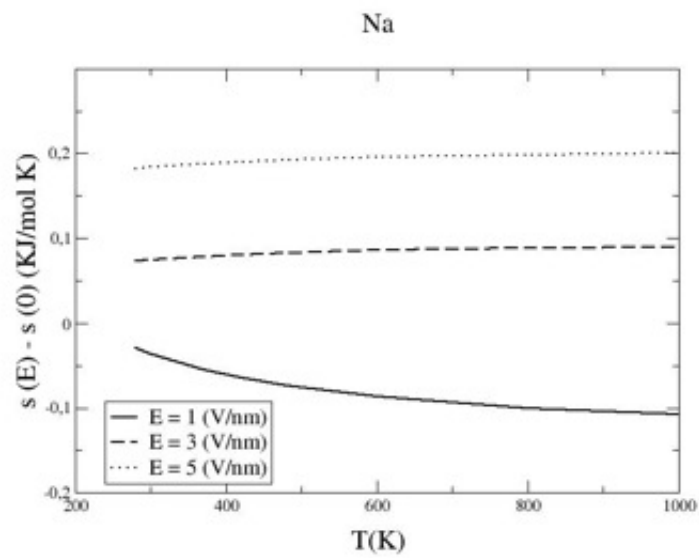
Figure 4.7: **Partial molar entropy shift of sodium ion.**
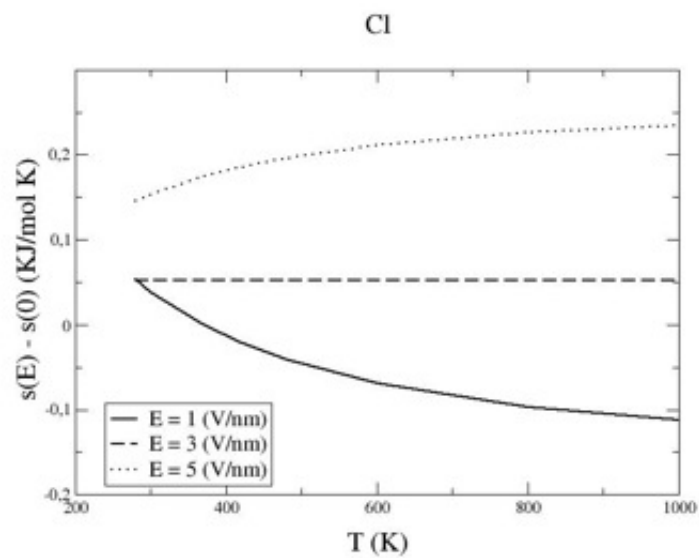
Figure 4.8: **Partial molar entropy shift of chloride ion.**

behavior must occur beyond $1\,\mathrm{V/nm}$ field strength, as evidenced by the change in the concavity of the chemical potential, partial molar energy and entropy due to the sign variation of three key model parameters ($\Delta c'_{V0}, \Delta v, R\ln\gamma$, see tables 4.1 and 4.2).

Table 4.1: Parameters of the QGE theoretical models for the sodium ion partial molar properties.

$T_0 = 300\,\mathrm{K}$	$\Delta u'_0$ (kJ/mol)	$\Delta c'_{V0}$ (kJ/mol K)	Δv (l/mol)	$R\ln\gamma$ (kJ/mol K)	δ_0	
1(V/nm)	15	- 0.095	- 0.057	- 0.101	0.6565	
3(V/nm)	62.9	0.021	0.025	0.083	0.6565	
5(V/nm)	110	0.022	0.082	0.167	0.6565	

Table 4.2: Parameters of the QGE theoretical models for the chloride ion partial molar properties.

$T_0 = 300\,\mathrm{K}$	$\Delta u'_0$ (kJ/mol)	$\Delta c'_{V0}$ (kJ/mol K)	Δv (l/mol)	$R\ln\gamma$ (kJ/mol K)	δ_0	
1(V/nm)	7.5	- 0.202	- 0.016	- 0.147	0.6565	
3(V/nm)	56	~ 0	0.021	0.043	0.6565	
5(V/nm)	119	0.109	0.090	0.216	0.6565	

In fact at $1\,\mathrm{V/nm}$ the ion partial molar (isochoric) heat capacity variation with respect to the zero field condition is negative, resulting in a partial molar entropy and energy decrease as temperature increases. Such heat capacity behavior is associated to the partial molar volume (Δv) and confinement entropy ($R\ln\gamma$) decrease with respect to the zero field condition, indicating more compact and ordered first solvation shells. At higher field intensity the enhanced watre polarization clearly provides less compact and ordered first solvation shells, resulting in increasing partial molar energy and entropy as temperature raises (i.e. positive partial molar heat capacity, volume and confinement entropy variations).

These thermodynamic results evidenced from the QGE model based on MD simulations, clearly point out that a relevant transition of the solvent molecular organization must occur in the range 1–$3\,\mathrm{V/nm}$.

In figure 4.9 we illustrate such solvent transition in the first solvation shells (i.e. within a 0.8 radius sphere centered on the ion) by showing the mean molecular electric moment along the external field direction as a function of the increasing field strength. The figure clearly shows that for all the cases considered the 0–1 V/nm range corresponds to a very efficient solvent polarization (i.e. a limited field increase provides a large polarization increase) while for field intensities beyond 3 V/nm a much less efficient polarization regime appears. Note that for both ions the switching the two polarization regimes occurs in the 1–3 V/nm range, well matching the thermodynamic switching range provided by the QGE model (see tables 4.1 and 4.2).
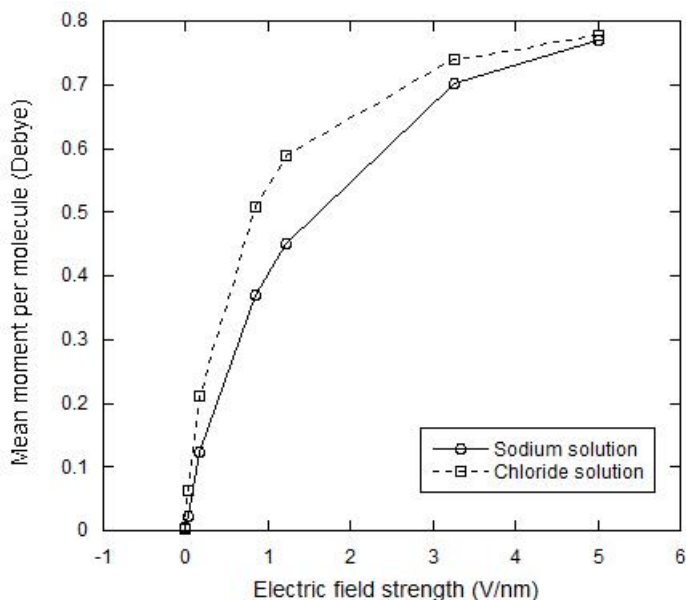
Figure 4.9: **Mean solvent molecular dipole along the external field direction, as obtained in the 0.8 nm radius sphere centered on the ion.**

4.4 Conclusions

The combined use of MD simulations and QGE theory allowed the construction of a detailed quantitative model of the thermodynamics of ionic solutions (chloride and sodium ion solution) in presence of an applied external (homogeneous) electric

field.

Results showed that for both ionic solutions the 1–3 V/nm range corresponds to a switching between two thermodynamics regimes (see tables 1 and 2): a first one, within the 0–1 V/nm range, characterized by negative variations (with respect to the zero-field condition) of the ion partial molar volume, heat capacity and entropy and a second one, beyond 3 V/nm, associated to positive ion partial molar volume, heat capacity and entropy variations.

Such a behavior, reflecting a similar switching between two polarization regimes of the ion first solvation shells (see figure 9), reveals the effects of the balance between the ionic and external fields. When the external field is unable to destroy the (zero-field) solvent organization around the ion (within the 0–1 V/nm range), the solvent polarization provides more compact and ordered first solvation shells. On the other hand the opposite behavior arises when the external field is strong enough to significantly break the solvent organization around the solute.

THEORETICAL AND COMPUTATIONAL CHARACTERIZATION OF THE EFFECT OF HOMOGENEOUS ELECTRIC FIELDS IN ZWITTERIONIC MICELLE

Summary

Micelles belong to the class of promising colloidal nanocarriers for the targeting of poorly water soluble and amphilic drugs. In the present study, a zwitterionic micelle has been choosen as a simple molecular vector tipically used in nano-medicine applications. We specifically investigate the behavior of the micelle (N,N-dimethyl-tetradecylamine-N-oxide) in water under the effect of an external electric field by using Molecular Dynamics simulations. Such an approach allows to study the structural properties of the micelle and to underline the thermodynamic effects induced by homogeneous electric field.

5.1 Introduction

The atomic-scale and cutting edge field of nanotechnology which is considered to lead us to the next industrial revolution is likely to have a revolutionary impact on the way things will be done, designed and manufactured in the future.[84] Nanotechnolgy is entering into all aspects of science and technology including, but not limited, to aerospace, agriculture, bioengineering, biology, energy, the environment, materials, manufacturing, medicine, military science and technology. It is based on bottom-up (atomic and molecular) approach, which starts from nano- or sub-nanoscale objects (namely, atoms or molecules) to build up nanostructures.

Nanotechnology is an area of science devoted to the design, construction, and utilization of functional structures on the nanometer scale (often 100 nm or smaller). At the nanoscale, the properties of materials often differ from those of the corresponding bulk materials. In fact, fundamental characteristics of a given material can be precisely controlled by nanotechnology without changing its chemical composition such as melting point, magnetic properties, or even a characteristic as basic as color.[85] There are numerous applications for nanotechnology. Among them, the treatment, diagnosis, monitoring and the control of biological systems has recently been referred to as "Nanomedicine" by the National Institute of Health.[86]

Nanomedicine may involve a number of different types of nanodevices, including nanoparticles, nanomachines, nanofibers, sensors, and other nanoscale microfabrication-based entities.[87] The nanomedicine-based diagnostics developed to date include gold nanoshells, iron oxide nanocrystals, and quantum dots. Indeed, although these nanoparticles have provided new opportunities for diagnosing cancer, their practical application has been limited by problems with toxicity, instability, and lack of selectivity for the disease site.

In recent years, researchers have sought to overcome these limitations by physically or chemically anchoring biocompatible polymers on the surfaces of diagnostic nanomedicines. The surface modification of nanoparticles with hydrophilic polymers such as poly(ethylene glycol) (PEG) reduces the interfacial energy in an aqueous environment, thus preventing unwanted aggregation due to secondary interactions between nanoparticles. In addition, the surface decoration of nanoparticles with hydrophilic polymers may minimize recognition by proteins and cells

in the body, allowing the nanomedicine to circulate in the blood for a longer period of time and increasing the possibility that it will reach the target site. In the context of nanomedicine-based therapeutics, effective cancer therapy requires drug delivery to cancer tissues, meaning that a drug delivery system should hold the anticancer drug in the blood and then allow a burst or continuous drug release at the cancer.[88] For this purpose, a variety of lipid-based drug delivery systems have been developed in the form of liposomes and lipid-core micelles.

Over the past decade, researchers have sought to develop cancer therapeutics involving drug delivery by a combination of nanotechnology and polymer chemistry. Most of the polymers used for these systems are biocompatible and/or biodegradable. The drug is typically either dispersed within the polymeric nanoparticle or conjugated to the polymeric back-bone.[23]

Among polymers used, polymer micelles have received a great deal of attention as colloidal carriers of poorly water-soluble and amphiphilic drugs. Polymeric micelles, which were introduced by Ringsdorf in 1984,[89] are formed by amphiphilic block copolymers in aqueous solution. The capacity of polymeric micelles to increase the solubility of hydrophobic drugs stems from their unique structural composition, which is characterized by a hydrophobic inner core sterically stabilized by a hydrophilic shell. A polymeric micelle can serve as a nanosized container into which drugs can be incorporated by chemical, physical, or electrostatic interactions.

The use of polymeric micelles as drug carriers offers several advantages over conventional dosage forms: they protect drugs from harsh biological environments (e.g. low pH and hydrolytic enzymes), and the small size of polymeric micelles (10-100 nm in diameter) should facilitate drug targeting and reduce the side effects of chemotherapy. The stability of the drug is also increased through micelle incorporation. Furthermore, undesirable side effects are lessened, as contact of the drug with inactivating species, such as enzymes present in biological fluids, are minimized, in comparison with free drug. They can be prepared in large quantities easily and reproducibility. By far the most important feature of micellar deliver systems, which distinguish them from other particulate drug carriers, lies in their small size ($\sim$ 10 to 30 nm) and the narrow size distribution. Another beneficial aspect of polymeric micelles for drug delivery is their relatively lengthy retention time in circulation.

Another type of drug delivery systems could be possibly based on stimuli-responsive polymers, which sense a change in a specific variable (as for example an electric field) and activate the delivery. Harada et al.[90] have found a remarkable elevation of the lysozyme activity through the inclusion into the polyion complex (PIC) micelles, thus achieving for the first time the drastic switching of enzymatic reactivity synchronizing with the application of a pulse electric field.

In this specific context, we have studied as model system the zwitterionic micelle (N,N-dimethyl-tetradecylamine-N-oxide) by using molecular dynamics simulations (MD).

Micellar aggregates have been probed by a number of experimental methods, such as NMR,[91] EPR,[92] small angle neutron scattering,[93] light scattering,[94] and diffusion measurements.[95] None of these methods provide enough information to deduce a complete structure or even provide conclusive evidence about a proposed structure. However, they can rule out certain suggestions and they give direct evidence about certain structural and dynamic properties of the system. Theoretical methods, among which Monte Carlo and MD, have the advantage that they can provide a more detailed information than experiments. Since these systems are complicated, however, any successful theoretical treatment involves simplifications that are not immediately justifiable. It is therefore important to compare with experimental results and adjust the model if it fails to reproduce them.

Aim of the present study is to thermodynamically characterize the zwitterionic micelle under the effect of an external static electric fields by using MD simulations.

The chapter is organized as follows: The construction of the model system and the simulation run are outlined. A brief description of methods utilized to extrapolate geometrical informations from simulated system are given. Finally, we report an accurate structural description of the micelle as provided by MD simulations and the evaluation of electric field effects.

5.2   Methods

The model system in the present study comprises 55 amphiphilic monomers of TDDNO (N,N-dimethyl-tetradedecylamine-N-oxide), and 14123 (simple point charge) SPC water molecules. This large number of water molecules allows a more accurate simulation of the environment of the micelle. The aggregation number of 55 has

been determined experimentally by the "critical micelle concentration" (CMC), that is defined as the concentration of surfactants above which micelles are spontaneously formed. The micelle was constructed so that the innermost methyl group in each of the hydrophobic tails was placed close to the center of a sphere with a radius of $\sim 2\,\text{nm}$, and the remainder of the monomer extending outward. The chemical structure of the TDDNO surfactant molecule is shown in Figure 5.1. Partial charges on the atoms of the headgroup are shown in Table 5.1.

Table 5.1: Surfactant headgroup charges

atom	charge (atomic units)
CH_2	0.0268
N	0.6164
CH_3	0.0314
O	-0.7062
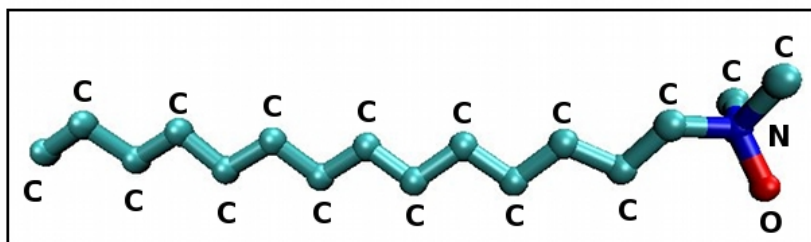
Figure 5.1: **TDDNO surfactant used in MD simulations. (hydrogen atoms not shown)**

Molecular Dynamics simulations, in the NVT ensemble, were performed using the GROMACS software package[96] and with the GROMOS96 43a1 force field.[29] Water was modeled by the SPC model.[76] A nonbonded cutoff was fixed at 9.0 Å and all long-range electrostatic forces were calculated using the Particle Mesh Ewald method.[83] The temperature was kept constant by using the isokinetic temperature coupling.[97]

The system was then subjected to further energy minimization and thermalization, letting the micelle to reach a stable condition, a more compact structure and also to allow the water molecules to relax around the lipids (Figure 5.2).

In this step roto-translational movements of the micelle were allowed, leading to a slight geometrical shift with respect to the center of the simulation box. Thermalization was carried out in three steps: 1) a sequence of simulations of 60 ps up to a temperature of 200 K; 2) a simulation of 600 ps at 250 K; 3) a simulation of 600 ps at 300 K. The final density of entire system was 1000 g/l and the final periodic cubic box of dimensions $76.6 \times 76.6 \times 76.6$ Å. Finally, a set of simulations were carried out using LINCS[98] to constrain the bond lengths in the lipids, with a time step of 2 fs, and with a time length of 50 ns, considered as a suitable time to study the dynamical properties of the system. Simulations were performed at room temperature (T = 300 K) and using 5 external electric fields conditions $(10^3 - 10^4 - 10^5 - 10^6 - 10^7 \, \text{V/m})$, typical of the micro and nano-pulses electric field applications. A reference simulation was performed at 300 K, with a temporal lenght of 50 ns, without an external electric field applied. During the production time, free rotation of the micelle was allowed while its centre of mass was frozen.

5.3 Results and Discussion

5.3.1 Analysis of the Micelle Structure in absence of electric field

In previous studies[99, 100, 101] the size and shape of micelles were evaluated by their radius of gyration and principal moments of inertia. In the present study the geometrical structure of the micelle and fluctuations are studied by means of the principal geometric axes obtained by diagonalization of the 3*3 Covariance Matrix of the system at each MD frame, whose elements are the covariances of the x, y and z atomic cartesian coordinates of the lipidic ensemble. The eigenvectors correspond to the geometrical principal axes of the micelle (geometrically approximated by an ellipsoid), while the squares root of the three eigenvalues provide a measure of axes lengths. The results are consistent with the conventional static picture of a spherical micelle with hydrophilic heads out and hydrophobic core inside. The relative magnitude of the three principal components, 1.33:1.14:1, in
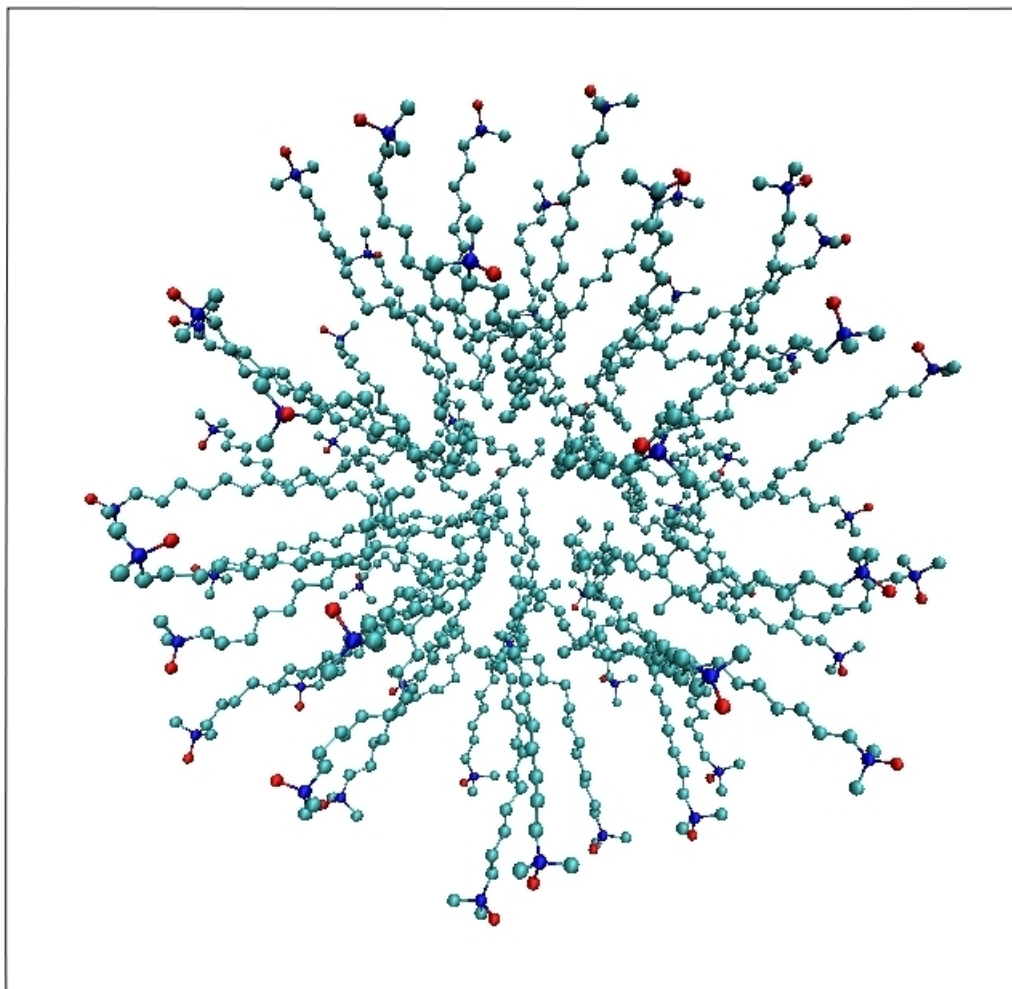
Figure 5.2: **Structure of the micelle. (water molecules are not shown)**

absence of external electric field, implies that the micelle is roughly spherical with individual surfactant molecules adopting various nonlinear conformations, mainly in the hydrophilic segment, thereby leading to the overall compact globular shape of the micelle aggregate.

The time-behaviour of the micelle eigenvalues, shown in Figure 5.3, indicates that the micelle structure maintains its ellipsoidal shape and a good structural stability over the whole 50 ns time-length: the mean distance between the micelle centre of mass and micelle heads results 1.825 ±0.026 nm. It is also possible to obtain the size of the conformational space of the micelle by representing the projection of the equilibrated trajectory on the plane of the first and second (or third) eigenvalue. Figures 5.4 and 5.5 show that the structure remains stable and confined in a single closed region with well defined border, high diffusivity, and high energy barriers.
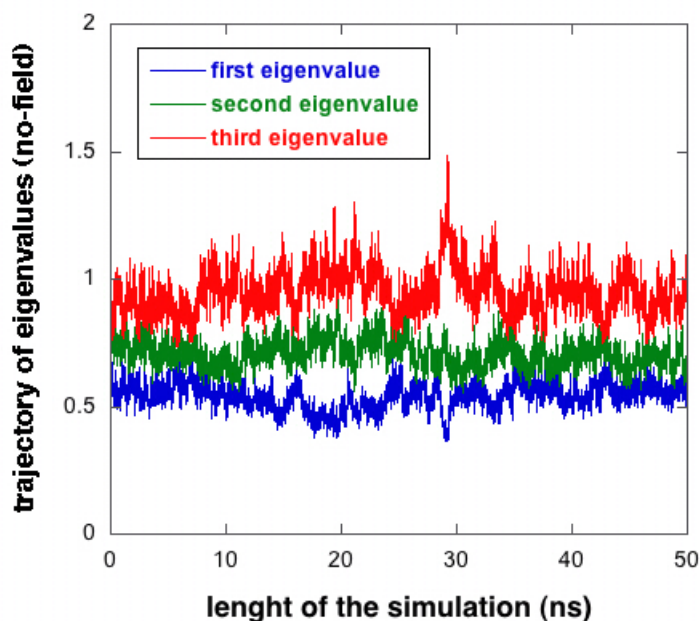
Figure 5.3: **Eigenvalues trend during all the simulation.**
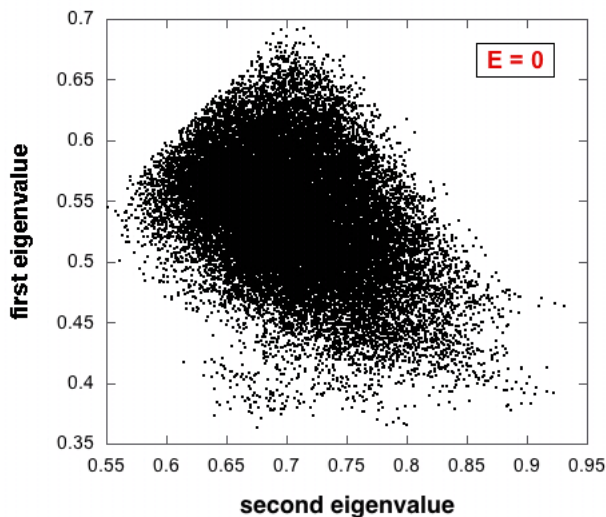
Figure 5.4: **Projection of the equilibrated trajectory on the plane of the first and second eigenvalue.**

5.3.2   Density of components in absence of electric field

In this section a description of the water-micelle ensemble is presented in order to characterize the micelle in absence of external electric fields. This has been carried out by studying the density distribution of the selected atoms in the system that also provides informations about its composition. A radial density plot (Figure 5.6) was constructed by calculating the distance of the selected atoms from the micelle center of mass. The figure shows that hydrophobic tails density rapidly decreases between 13 and 22 Å, while the hydrophilic heads density rapidly decreases between 18 and 25 Å. Moreover the water density is zero within 12 Å from the micelle center of mass and gradually increases up to 23 Å. This is followed by a broad plateau up to 35 Å, during which a gradual decrease in the density occurs. The gradual decrease in the water density from 23 to 35 Å suggests an influence of the micelle on the adjacent bulk solvent. The hydrophilic heads, as shown in Figure 5.6, are distributed between 12 and 25 Å. Both the hydrophilic head and water go to zero at ~ 12 Å from the micelle center of mass. This result also agrees with those reported
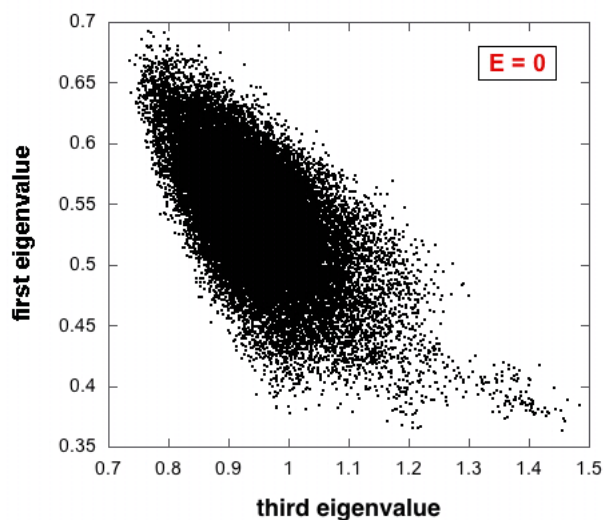
Figure 5.5: **Projection of the equilibrated trajectory on the plane of the first and third eigenvalue.**

by MacKerrell.[102] This analysis shows that the micelle can be subdivided in three zones (Figure 5.7): an internal zone (< 1.6 nm), containing the hydrophobic core, an external zone (> 1.8 nm) containing water molecules and a transition zone, where polar heads are distributed.

5.3.3   Electric potential profile in absence of electric field

It is also interesting to investigate the electric potential profile along micelle's radial direction, whose gradient represent the local field acting on the water-micelle system. This has been carried out by the classical law of Coulomb, calculating the sum of electric potentials on all atoms of the box, starting from the micelle center of mass and moving radially toward the left box. Firstly we estimated the electric potential profile along three principal axes of the micelle as a function of the distance from the micelle center of mass, but without the application of an external electric field. The figures clearly show a direct measure of potential difference of about 0.8 V, always the same along three axes of the micelle, between
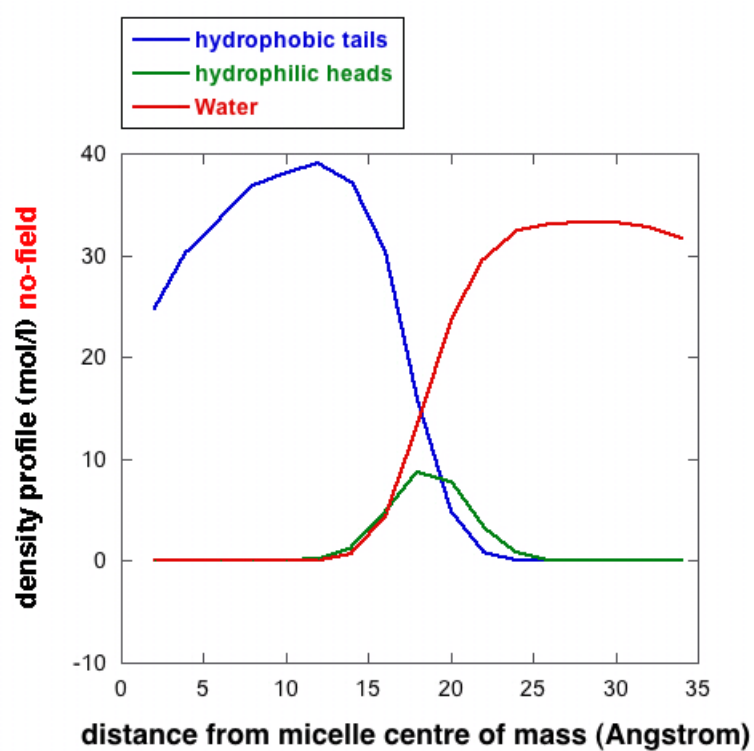
Figure 5.6: **Density of selected atoms as a function of distance from the micelle center of mass.**
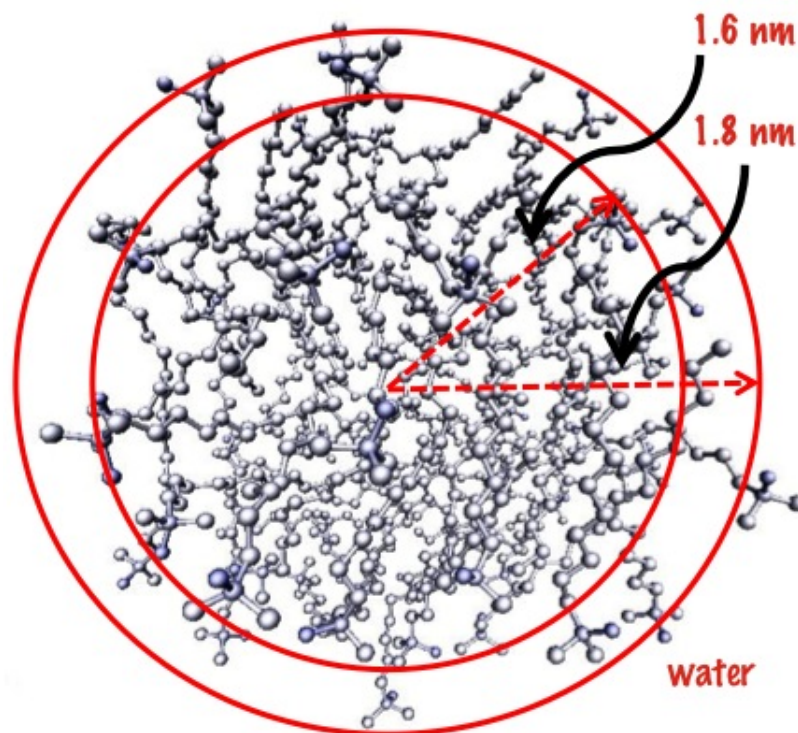
Figure 5.7: **The micelle subdivides in three zones.**

the inner core of the micelle and the external environment (Figures 5.8-5.10).
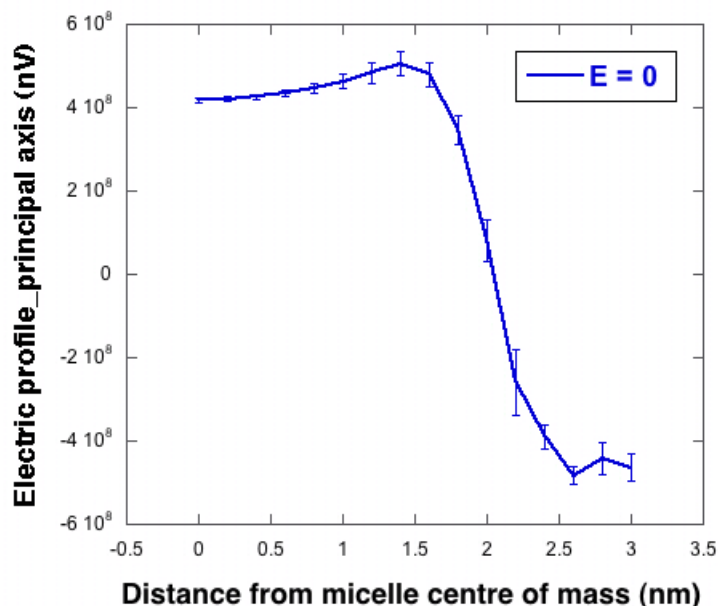
Figure 5.8: **Electric potential profile along principal axis of the micelle.**

5.3.4 Analysis of the Micelle Structure in electric field

To analyse the structural properties of the micelle with respect to the perturbed state, we have been carried out the same kind of analysis. From Figures 5.11 and 5.12 it is possible to observe such as the trajectory of the eigenvalues remains also unchanged with the presence of increasing external electric fields. Subsequently we calculated mean of three eigenvalues for different electric field intensities by comparison with the zero state field. In Figure 5.13 it is worth to note that for all the external electric fields intensities we obtained, within the thermal noise, an identical behaviour without evident structural changes. While Figures 5.14 and 5.15 show the size of the conformational space of the micelle at 10^5 V/m and Figures 5.16 and 5.17 show the size of the conformational space of the micelle at
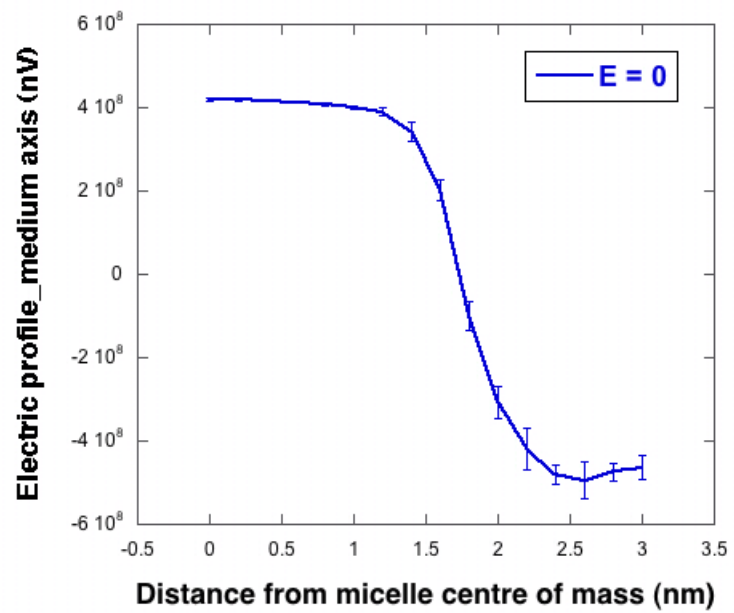
Figure 5.9: **Electric potential profile along medium axis of the micelle.**
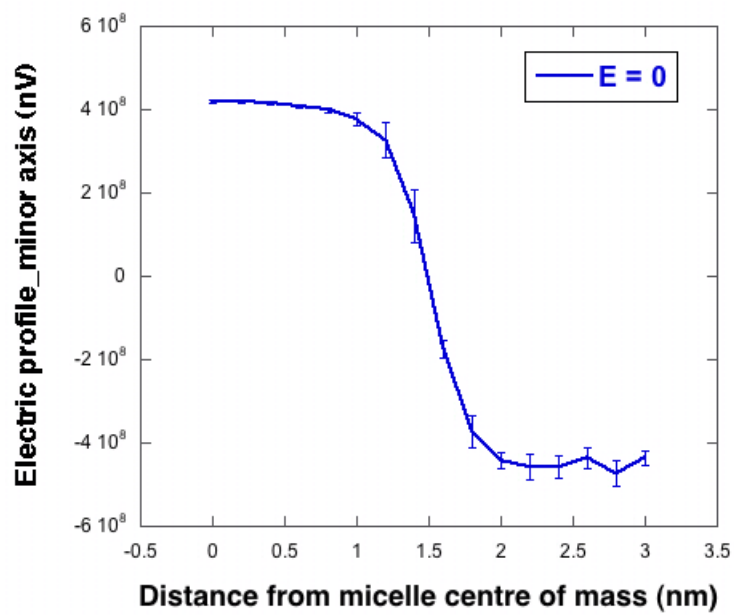
Figure 5.10: **Electric potential profile along minor axis of the micelle.**

10^6 V/m. These figures confirm again the stability of the micelle in presence of an applied external electric field.
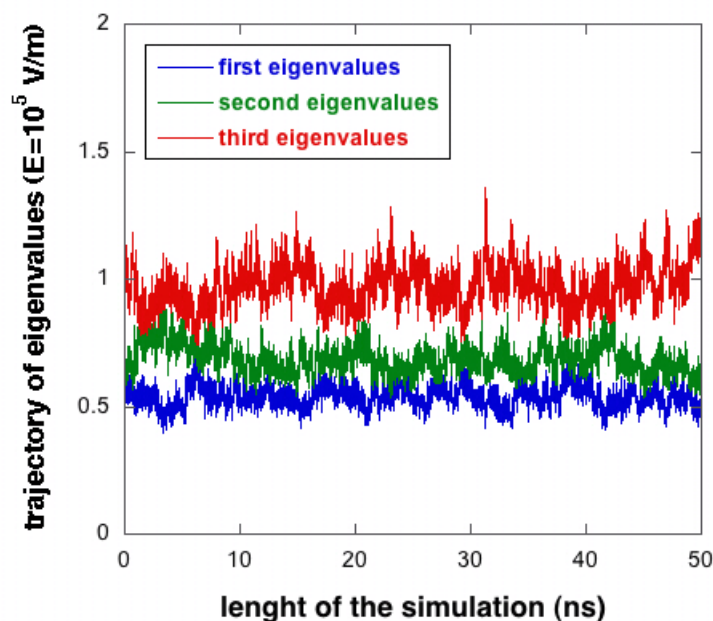
Figure 5.11: **Eigenvalues trend during all the simulation in E field.**

5.3.5   Density of components in electric field

A more exhaustive analysis seems to be interesting in regard to the density distribution of the system under strong external fields. Only fields of 10^5 V/m or larger were able to provide decrease in the water density profile that is observable in Figure 5.18. From the figure it is possible to see that the water density is zero within 14 Å from the micelle center of mass compared to the unexposed water density that is zero within 12 Å, resulting in a reduction of water molecules inside the micelle's hydrophobic core. Focusing the attention on interaction mechanisms among the imposed external electric fields and the water inside the micelle (i.e. for distance < 1.8 nm), in Figure 5.19 we report the water density ratio between
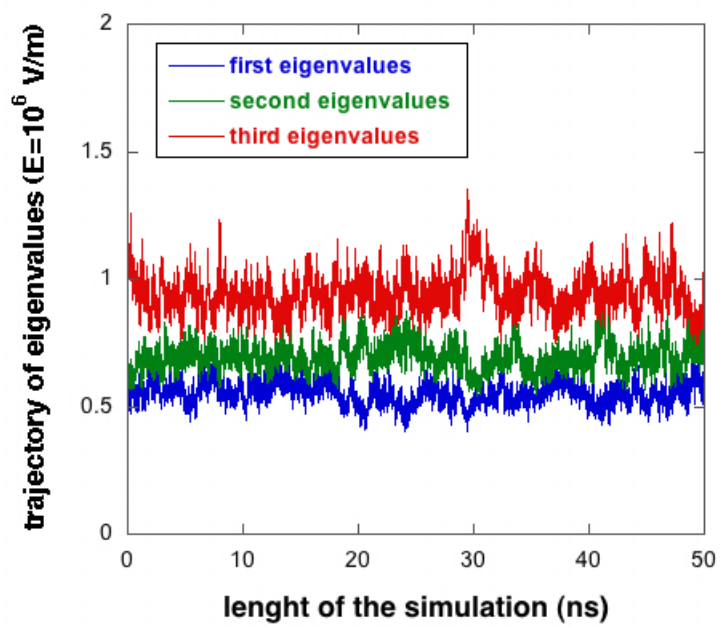
Figure 5.12: **Eigenvalues trend during all the simulation in E field.**
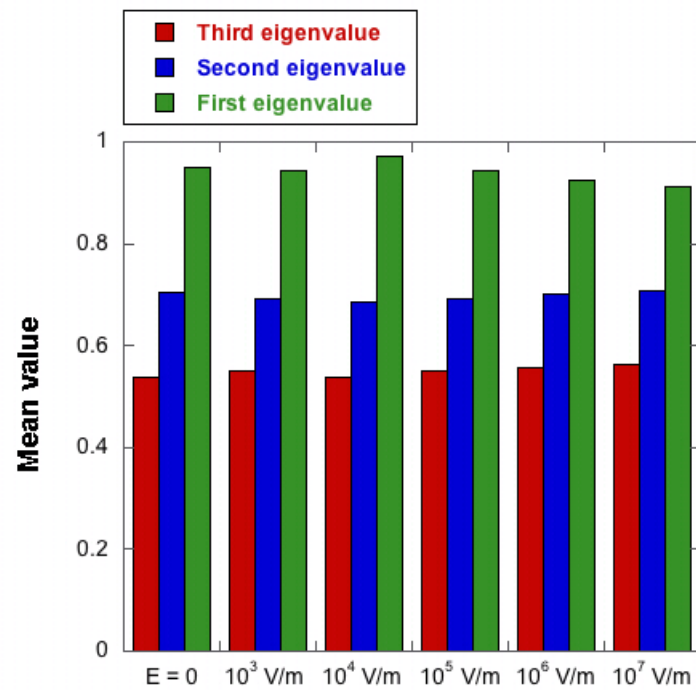
Figure 5.13: **Average number of three eigenvalues as a function of the increasing field strength.**
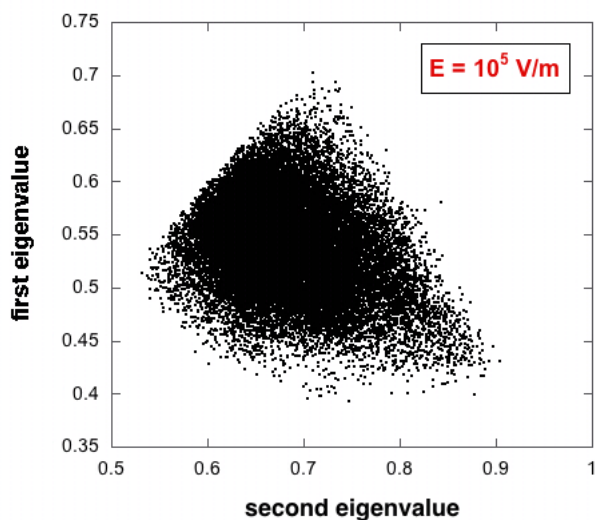
Figure 5.14: **Projection of the equilibrated trajectory on the plane of the first and second eigenvalue in E field.**

exposed and unexposed conditions, showing clearly a decrease of the water density in the presence of external electric fields.

It is worth to note that the presence of external electric fields greater than 10^4 V/m involves an evident variations in the thermodynamic behavior of the water: an overall shift in Helmholtz free energy up to $4 - 5$ kJ/mol is obtained with these exposures via: $A = -kT \log \rho$. Such results suggest that water molecules and, in principle, also other type of solute molecules, are pushed away from the micelle's hydrophobic core when an external electric field is applied. On the other hand, in unexposed conditions, water molecules stay inside the micelle's core. To gather informations about the total number of water molecules within a given distance from the micelle centre of mass and its variations when an external electric field is applied, we can integrate the density curves hence obtaining the values reported in Figure 5.20. To prove as the electric field influences the behavior of water molecules we report another Figure 5.21 where it is possible to see the distribution of the water molecules number inside the micelle core in the presence or in the absence of the electric field. It is interesting to observe that electric fields
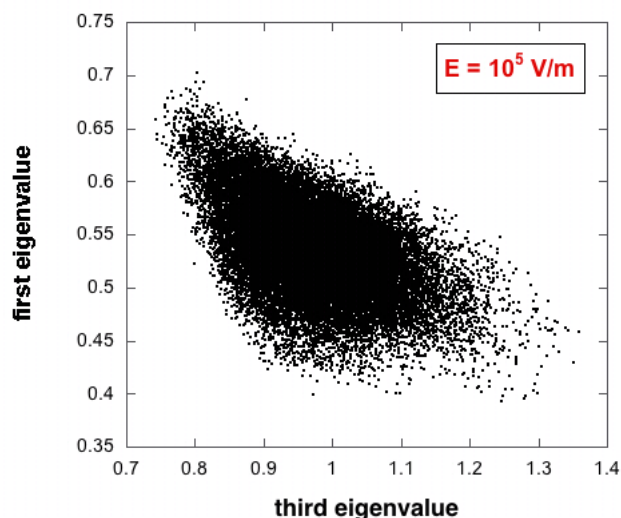
Figure 5.15: **Projection of the equilibrated trajectory on the plane of the first and third eigenvalue in E field.**

beyond a certain threshold (10^5 V/m) produce up to 20 % variation in the number of water molecules inside the micelle core. To note that the electric field influences on water molecules displacement up to a distance of 1.6 nm (the border region between the hydrophilic part of micelle monomers and the external environment) is statistically significant (t and Wilcoxon tests for trend and two way Anova with p<0.05).

5.3.6   Electric potential profile in electric field

In Figures 5.22-5.24 we calculated the electric potential profile along three axes of the micelle, under the influence of an external electric fields at various intensity, but essentially the profile of the electric potential remains always the same with a difference of potential of about 0.8 V between the core of the micelle and the external medium. The other way round this result cannot provide a clear picture of the external field influence on atomic charge displacement, except for very high exposure condition (10^7 V/m). The latter case corresponds, experimentally
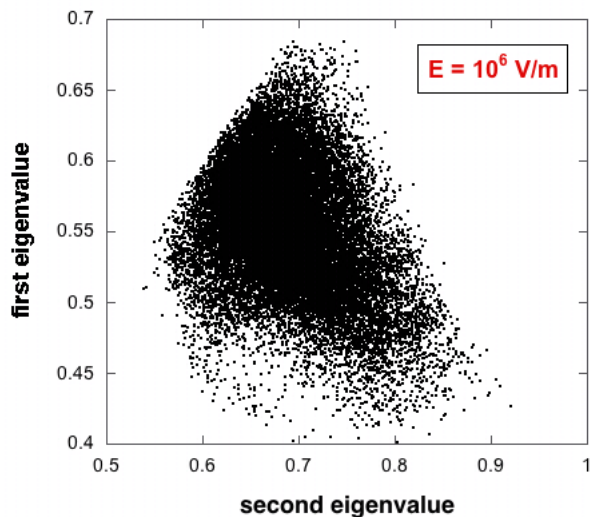
Figure 5.16: **Projection of the equilibrated trajectory on the plane of the first and second eigenvalue in E field.**

speaking, to the application on biological sample of high electric pulses typical of nano-poration techniques. Nevertheless the presence of a positive electrostatic potential in the interior micelle and the fast transition toward negative values as the external environment is reached. This kind of result could be important for describing the transmembrane transport of small (charged) solute molecules (i.e. drug molecules).

5.4   Conclusions

In the present study, a structural characterization of a water-micelle system in presence of an external electric field has been extensively investigated by the use of MD simulations coupled to a molecular detailed approach. In the course of a 50 nanosecond molecular dynamics simulation, it has been determined that a zwitterionic micelle composed of 55 amphiphilic monomers TDDNO (N,N-dimethyl-tetradedecylamine-N-oxide), and 14123 SPC water molecules is stable. Of the micellar characteristics evaluated in this work, none had significant deviation over
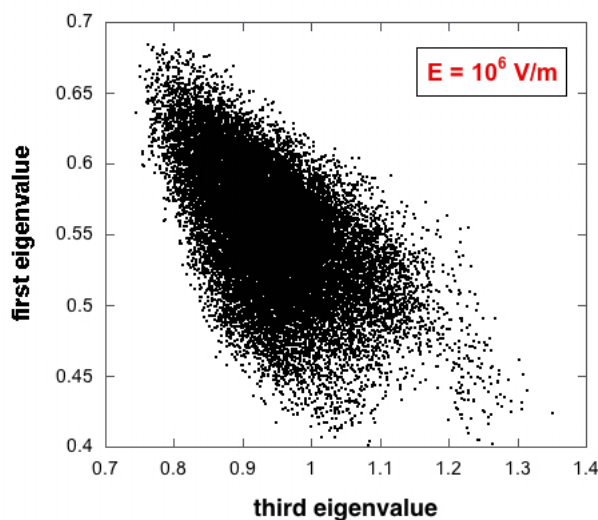
Figure 5.17: **Projection of the equilibrated trajectory on the plane of the first and third eigenvalue in E field.**

time of the simulation except for the water molecules distribution inside the micelle's environment. All micellar structural quantities were stable throughout the simulation. Evaluation of the micelle shape by investigation of the 3*3 Covariance Matrix of the system revealed that the micelle is not completely spherical, but is slightly ellipsoidal. This result is always the same with no evident structural modifications when an external electric field of increasing intensities is applied. On the other hand a direct effect on water molecules distribution inside the micelle's core and a change of thermodynamic properties of the system is evidenced: for an external electric field of high intensities ($E=10^5$ V/m) is observed a significant leak of water molecules on the outside of the micelle, hence leaving a 'more' hydrophobic core. The opposite behavior arises at the zero field condition, resulting in a capture of water molecules inside the micelle's core. Another preliminary result is the calculation of the electric potential profile along the micelle's radial direction that furnishs a measure of the potential difference of about 0.8 V between the micelle's core and the external environment without or with the external electric field. These findings, in principle, could be exploited, in the diverse fields
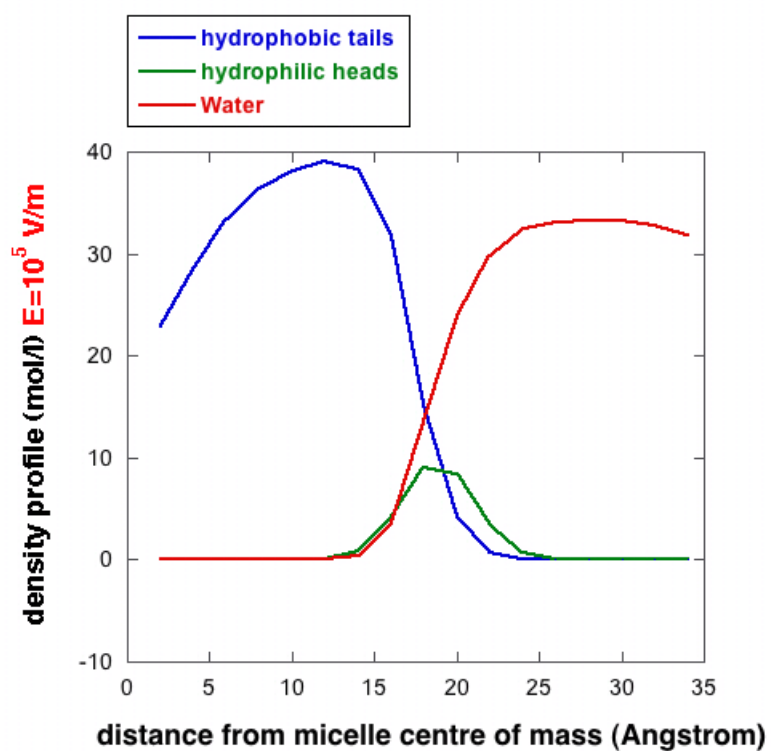
Figure 5.18: **Density of selected atoms as a function of E field.**
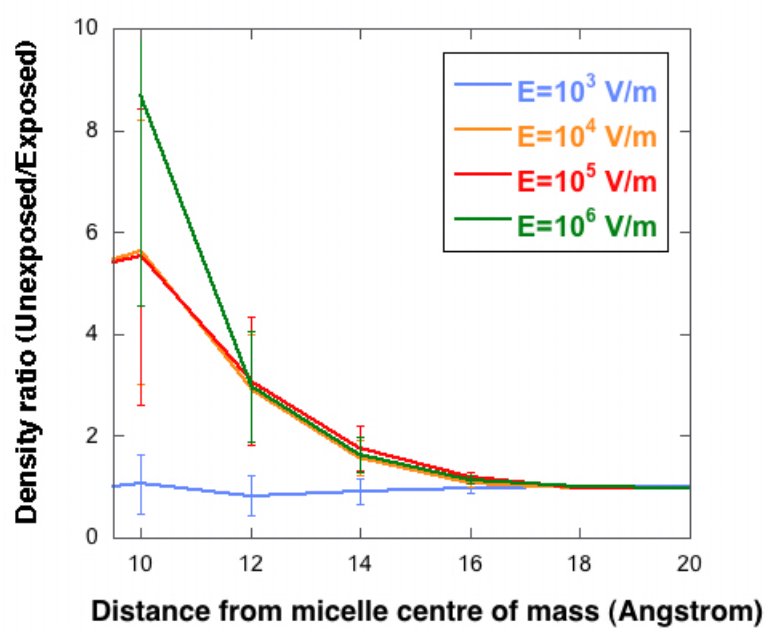
Figure 5.19: **Density ratio between unexposed and exposed density profiles.**
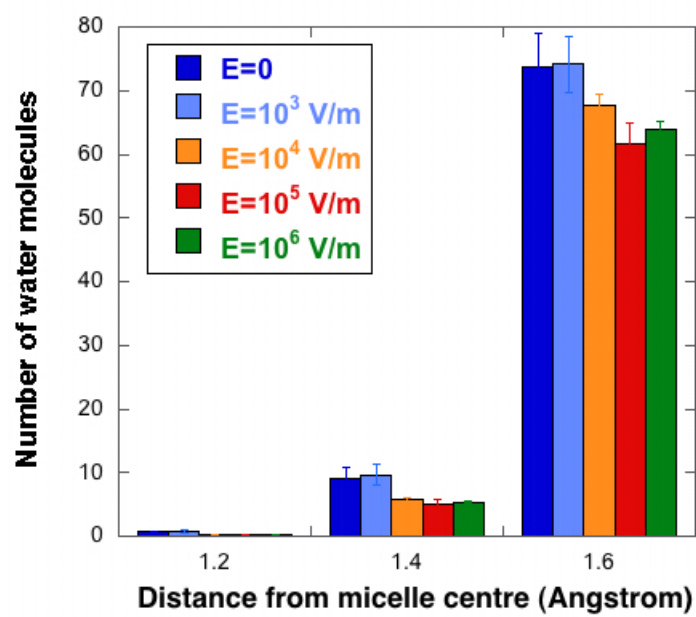
Figure 5.20: **Mean number of water molecules at different distances from the micelle centre of mass.**
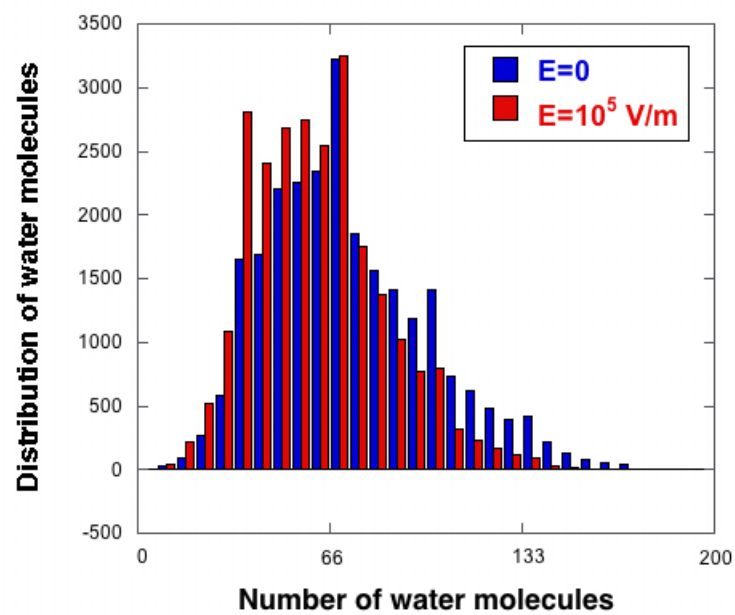
Figure 5.21: **Distribution of the water molecules number inside the micelle core induced by the electric field.**
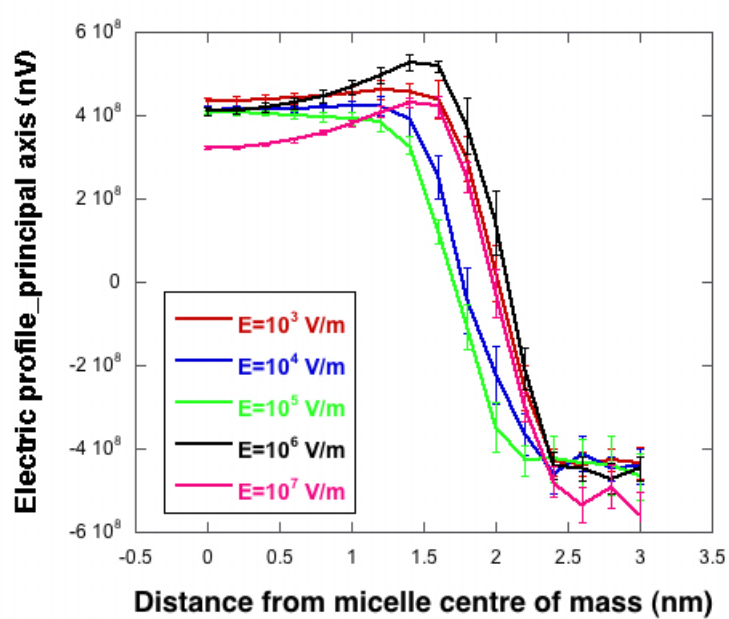
Figure 5.22: **Electric potential profiles along principal axis of the micelle, for different electric field intensities.**
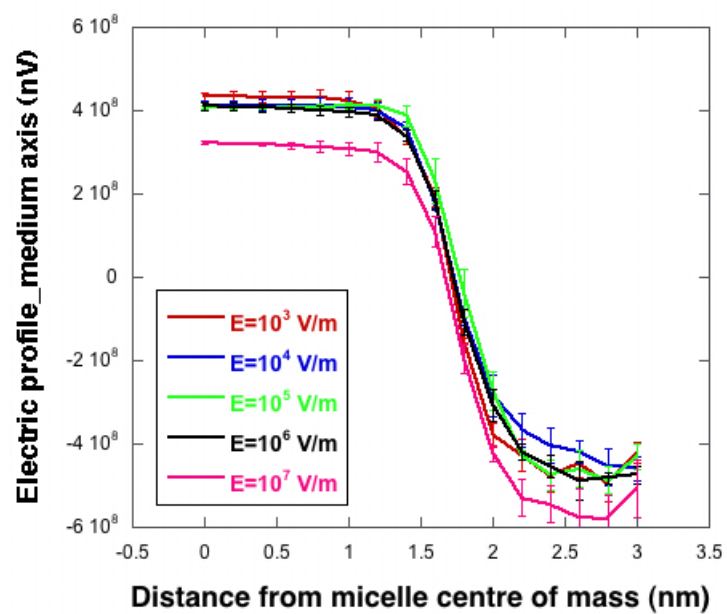
Figure 5.23: **Electric potential profiles along medium axis of the micelle, for different electric field intensities.**
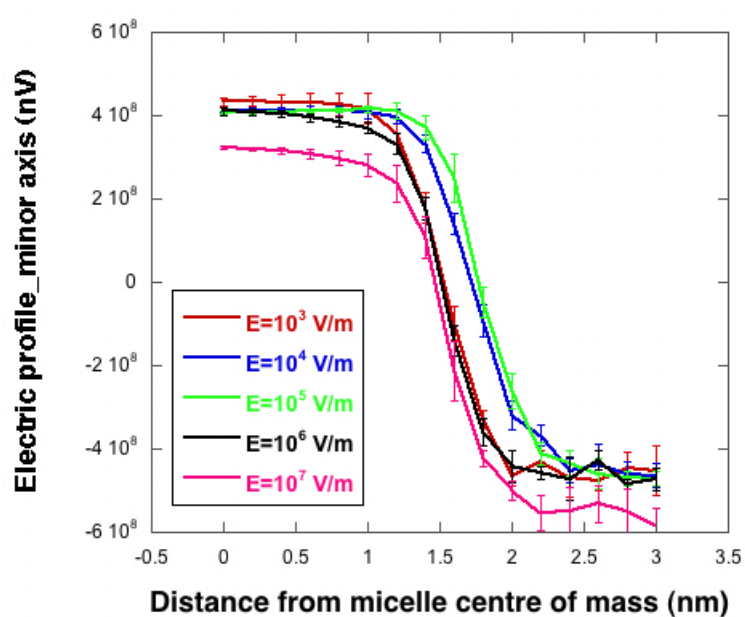
Figure 5.24: **Electric potential profiles along minor axis of the micelle, for different electric field intensities.**

of nano-medicine applications, to modelize engineered nano-structure capable to reversibly entrap small amounts of drug solute(i.e. increase the solubility of hydrophobic drugs) dispersed in the water.

SIX

CONCLUSIONS

In the present research activity, the external electric field action on microscopic structures was studied by both theoretical and computational methods, in order to obtain a deeper insight into the interaction occurring at the molecular and macromolecular levels of the biological scale of complexity.

The comprehension of the basic molecular mechanisms is indeed extremely important in biophysical research, since it is evident that whatever observable effect at the macroscopic scale is the result of electric interactions that take place at atomic level.

Molecular simulations have been used to investigate the dynamic behavior and functioning of molecules in their own realistic environment, both in physiological condition and under exposure to external electric field. Such an approach allowed the observation of electric field action on microscopic structures in an accurate and rigorous way, providing a realistic description of the interaction occurring at the atomic level.

The theoretical approach of the quasi-Gaussian entropy (QGE) theory has been applied in order to treat molecular systems of biological interest under the effect of external electric fields. Such a theory, characterizing the complete thermodynamic behavior by the distribution function of a macroscopic property, tackles the long standing problem of the calculation of the configurational (multidimensional) partition function, which is a high-dimensional integral, from a different viewpoint.

In the first part of this thesis we extended and used the QGE theory with

classical molecular dynamics (MD) simulations in order to obtain an accurate description of the thermodynamics of dilute ionic solutions (chloride and sodium ion solutions) under the effect of external (static) electric fields. Results showed that for both ionic solutions the 1–3 V/nm range corresponds to a switching between two polarization regimes of the ion first solvation shells: a first one, within 0–1 V/nm, characterized by a very efficient solvent polarization that provides more compact and ordered first solvation shells; while a second one, beyond 3 V/nm, characterized by a less efficient solvent polarization that breaks the solvent organization around the solute.

In the second part of this thesis a structural characterization of a water-micelle system in the presence of an external electric field has been extensively investigated by the use of MD simulations. Evaluation of the micelle structure by investigation of the 3*3 Covariance Matrix of the system revealed that the micelle is stable and slighly ellipsoidal in both the unexposed and exposed conditions. Finally another important result is the loss of water molecules from inside the micelle, following the application of the external electric field. This effect of the electric field on the micelle could be relevant to design engineered nano-structures for the veicolation of drugs.

BIBLIOGRAPHY

[1] C. Polk and E. Postow. *Handbook of biological effects of electromagnetic fields*. CRC Press, United States of America, 1996.

[2] H. P. Schwan and K. R. Foster. R-f field interactions with biological systems: electrical properties and biophysical mechanisms. *Proc. IEEE*, 104(68), 1980.

[3] K. S. Cole. *Membranes, Ions, and Impulses*. University of California Press, Berkeley, 1972.

[4] H. P. Schwan and Morowitz H. J. Electrical properties of the membranes of the pleuropneumonia-like organism a. *Biophys. J.*, 2(395), 1962.

[5] H. E. Stanley and J. Teixeira. Interpretation of the unusual behavior of h_2o and d_2o at low temperatures: Tests of a percolation model. *J. Chem. Phys.*, 73(7), 1980.

[6] S. Sastry, P. G. Debenedetti, F. Sciortino, and H. E. Stanley. Singularity-free interpretation of the themodynamics of supercooled water. *Phys. Rev. E*, 53(6):6144–6154, 1996.

[7] S. Sastry, F. Sciortino, and H. E. Stanley. Limits of stability of the liquid phase in a lattice model with water-like properties. *J. Chem Phys.*, 98:9863, 1993.

[8] S. J. Suresh. A new lattice-based theory for hydrogen-bonding liquids in uniform electric fields. *J. Chem Phys.*, 122:134502, 2005.

[9] M. Kiselev and K. Heinzinger. Molecular dynamics simulation of a chloride ion in water under the influence of an external electric field. *J. Chem. Phys.*, 105(2):650–657, 1996.

[10] D.H. Jung, J.H. Yang, and M.S. Jhon. The effect of an external electric field on the structure of liquid water using molecular dynamics simulations. *Chem. Phys.*, 244:331–337, 1999.

[11] A. Vegiri and S.V. Shevkunov. A molecular dynamics study of structural transitions in small water clusters in the presence of an external electric field. *J. Chem. Phys.*, 115(9):4175–4185, 2001.

[12] S. V. Shevkunov and A. Vegiri. Electric field induced transitions in water clusters. *J. Mol. Struct. : THEOCHEM*, 593:19–32, 2002.

[13] W. Sun, Z. Chen, and S. Huang. Effect of an external electric field on liquid water using molecular dynamics simulation with a flexible potential. *J. Shanghai University*, 10(3):268–273, 2006.

[14] M.F. Toney, J.N. Howard, J. Richer, G.L. Borges, J.G. Gordon, O.R. Melroy, D.G. Wiesler, D. Yee, and L.B. Sorensen. Voltage-dependent ordering of water molecules at an electrode-electrolyte interface. *Nature*, 368:444–446, 1994.

[15] M.F. Toney, J.N. Howard, J. Richer, G.L. Borges, J.G. Gordon, O.R. Melroy, D.G. Wiesler, D. Yee, and L.B. Sorensen. Distribution of water molecules at ag(111)/electrolyte interface as studied with surface x-ray scattering. *Surf. Sci.*, 335:326–332, 1995.

[16] K. A. Dill and P. J. Flory. Molecular organization in micelles and vesicles. *Proc. Natl. Acad. Sci. U.S.A.*, 78(676), 1981.

[17] K. A. Dill, D. E. Koppel, R. S. Cantor, J. D. Dill, D. Bendedouch, and S. Chen. Molecular conformations in surfactant micelles. *Nature*, 309:42–45, 1984.

[18] M. C. Woods, J. M. Haile, and J. P. O'Connell. Internal structure of a model micelle via computer simulation. 2. spherically confined aggregates with mobile head groups. *J. Phys. Chem.*, 90(9):1875–1885, 1986.

[19] J. C. Shelley, M. Sprik, and M. L. Klein. Molecular dynamics simulation of an aqueous sodium octanoate micelle using polarizable surfactant molecules. *Langmuir*, 9(4):916–926, 1993.

[20] J. J. Wendoloski, S. J. Kimatian, C. E. Schutt, and F. R. Salemme. Molecular dynamics simulation of a phospholipid micelle. *Science*, 243(4891):636–638, 1989.

[21] T. Wymore, X. F. Gao, and T. C. Wong. Molecular dynamics simulation of the structure and dynamics of a dodecylphosphocholine micelle in aqueous solution. *J. Mol. Struct.*, 485-486:195–210, 1999.

[22] D. P. Tieleman, D. van der Spoel, and H. J. C. Berendsen. Molecular dynamics simulation of dodecylphosphocholine micelles at three different aggregate sizes: Micellar structure and chain relaxation. *J. Phys. Chem. B*, (104):6380–6388, 2000.

[23] M. Jones and J. Leroux. Polymeric micelles - a new generation of colloidal drug carriers. *Eur. J. Pharmaceutics and Biopharmaceutics*, 48:101–111, 1999.

[24] M.P.Allen and D. J. Tildesly. *Computer simulation of liquids.* Oxford University Press, Oxford, 1989.

[25] D.Frenkel and B.Smit. *Understanding Molecular Simulation: From Algorithms to Applications.* Academic Press, Boston, 1996.

[26] W.F. Van Gunsteren and P.K. Weiner. *Computer simulation of biomolecular systems.* Escom Science, Leiden (NL), 1989.

[27] B.R. Brooks, R.E. Bruccoleri, B.D. Olafson, D. J. States, S. Swaminathan, and M. Karplus. Charmm: A program for macromolecular energy, minimization, and dynamics calculations. *J. Comput. Chem.*, 4:187–217, 1983.

[28] D.T. Nguyen S. J. Weiner, P.A. Kollman and D.A. Case. An all atom force field for simulations of proteins and nucleic acids. *J. Comput. Chem.*, 7:230–252, 1986.

[29] W.F. Van Gunsteren, S.R. Billeter, A.A. Eising, P.H. Hünenberger, P. Krüger, A.E. Mark, W.R.P. Scott, and I.G. Tironi. *Biomolecular Simulation: The GROMOS 96 Manual and User Guide*. Hochschulverlag AG an der ETH Zürich, Zürich, 1996.

[30] L. Verlet. Computer "experiments" on classical fluids. I. thermodynamical properties of lennard-jones molecules. *Physical Review*, 159(1):98, 1967.

[31] L. Verlet. Computer "experiments" on classical fluids. II. equilibrium correlation functions. *Physical Review*, 165(1):201, 1968.

[32] D. Beeman. Some multistep methods for use in molecular dynamics calculations. *J. Comput. Phys.*, 20:130, 1976.

[33] W. Gear. *Numerical initial value problems in ordinary differential equations*. Prentice Hall, ref. ed. edition, 1971.

[34] A. McCammon, B. Gelin, and M. Karplus. Dynamics of folded proteins. *Nature*, 267(5612):585–590, 1977.

[35] E. Barth T. Schlick and M. Mandziuk. Biomolecular dynamics at long timesteps: Bridgng the timescale gap between simulation and experimentation. *Annu. Rev. Biomol. Struct.*, 26:181–222, 1997.

[36] J.P. Ryckaert, G. Ciccotti, and H.J.C. Berendsen. Numerical integration of the cartesian equations of motion of a system with constraints: Molecular dynamics of n-alkanes. *J. Comput. Phys.*, 23:327, 1977.

[37] A. Amadei, G. Chillemi, M.A. Ceruso, A. Grottesi, and A. Di Nola. Molecular dynamics simulations with constrained roto-translational motions: Theoretical basis and statistical mechanical consistency. *J. Chem. Phys.*, 112(1):9–23, 2000.

[38] J.P. Van Den Berg H. Bekker and T.A. Wassenaar. A method to obtain a near-minimal-volume molecular simulation of a macromolecule, using periodic boundary conditions and rotational constraints. *J. Comput. Chem.*, 25:1037–1046, 2004.

[39] U. Essmann, L. Perera, M. Berkowitz, T. Darden, H. Lee, and L. Pedersen. A smooth particle mesh ewald method. *J. Chem. Phys.*, 103(19):8577–8593, 1995.

[40] H.J.C. Berendsen, J.P.M. Postma, W.F. van Gunsteren, A. Di Nola, and J.R. Haak. Molecular dynamics with coupling to an external bath. *J. Chem. Phys.*, 81(8):3684–3690, 1984.

[41] D. Brown and J.H.R. Clarke. Molecular dynamics computer simulation of polymer fiber microstructure. *J. Chem. Phys.*, 84(5):2858–2865, 1986.

[42] S. Nosè. Constant-temperature molecular dynamics methods. *Prog. Theor. Phys. Suppl.*, 103:1–46, 1991.

[43] W. Hoover. Canonical dynamics: Equilibrium phase-space distributions. *Physical Review A*, 31(3):1695, 1985.

[44] M.L. Klein G. J. Martyna and M.E. Tuckerman. Nosè hoover chains: The canonical ensemble via continuous dynamics. *J. chem. Phys.*, 97:2635–2645, 1992.

[45] A. Amadei, A. Linssen, and H.J.C. Berendsen. Essential dynamics of proteins. *Proteins*, 17(4):412–425, 1993.

[46] A.E. García. Large-amplitude nonlinear motions in proteins. *Physical Review Letters*, 68(17):2696, 1992.

[47] D.M.F. van Aalten, A. Amadei, A.B.M. Linssen, V.G.H. Eijsink, G. Vriend, and H.J.C. Berendsen. The essential dynamics of thermolysin: confirmation of the hinge-bending motion and comparison of simulations in vacuum and water. *Proteins*, 22(1):45–54, 1995.

[48] B.L. de Groot, D.M.F. van Aalten, R.M. Scheek, A. Amadei, G. Vriend, and H.J.C. Berendsen. Prediction of protein conformational freedom from distance constraints. *Proteins*, 29(2):240–251, 1998.

[49] D.M. van Aalten, D.A. Conn, B.L. de Groot, H. J.C. Berendsen, J.B. Findlay, and A. Amadei. Protein dynamics derived from clusters of crystal structures. *Biophys. J.*, 73:2891–2896, 1997.

[50] R. Abseher, L. Horstink, C.W. Hilbers, and M. Nilges. Essential spaces defined by nmr structure ensembles and molecular dynamics simulation show significant overlap. *Proteins*, 31(4):370–382, 1998.

[51] D.A. McQuarrie. *Statistical Mechanics*. Harper Collins Publisher Inc, New York, 1976.

[52] J.K. Kirkwood. Statistical mechanics of fluid mixtures. *J. Chem. Phys.*, 3:300–313, 1935.

[53] M. Mezei and D.L. Beverige. *Computer Simulations and Biomolecular Systems*. Ann. New York Academy of Sciences, New York, 1986.

[54] J.K. Patel, C.H. Kapadia, and D.B. Owen. *Handbook of statistical distributions*. Marcel Dekker, New York, 1976.

[55] N.L. Johnson, S. Kotz, and A.W. Kemp. *Univariate discrete distributions*. John Wiley Sons, New York, 1992.

[56] J.K. Patel and C.B. Read. *Handbook of the normal distribution*. Marcel Dekker, New York, 1982.

[57] T.L. Hill. *Statistical Mechanics*. McGraw-Hill Book Company, New York, 1956.

[58] J.E. Mayer and M.G. Mayer. *Statistical Mechanics*. Wiley, New York, 1940.

[59] G.A. Baker Jr. *Essentials of Padé approximants*. Academic Press, New York, 1975.

[60] G.A. Baker Jr. and J.L. Gammel. *The Padé approximant in theoretical physics*. Academic Press, New York, 1970.

[61] A. Amadei, M.E.F. Apol, A. Di Nola, and H. J.C. Berendsen. The quasi-gaussian entropy theory: Free energy calculations based on the potential energy distribution. *J. Chem. Phys.*, 104:1560–1574, 1996.

[62] J.K. Ord. *Families of frequency distributions*. Griffin, London, 1972.

[63] K.A. Dunning and J.N. Hanson. Generalized pearson distributions and nonlinear programing. *J. Statist. Comp. and Simul.*, 6(2):115–128, 1978.

[64] M.E.F. Apol, A. Amadei, and H. J.C. Berendsen. Application of the quasi-gaussian entropy theory to the calculation of thermodynamic properties of water and methane in the liquid and gas phase. *J. Chem. Phys.*, 104:6665–6678, 1996.

[65] J.P. Hansen and I.R. McDonald. *Theory of simple liquids*. Aca, New York, 1986.

[66] Norman Carnahan and Kenneth Starling. Equation of state for nonattracting rigid spheres. *J. Chem. Phys.*, 51(2):635–636, 1969.

[67] N.I. Johnson and S. Kotz. *Continuous Univariate Distributions*. Houghton Mifflin, New York, 1970.

[68] S.J. Suresh, A.V. Satish, and A. Choudhary. Influence of electric field on the hydrogen bond network of water. *J. Chem. Phys.*, 124(7):074506–074506–9, 2006.

[69] A. Amadei, M.E.F. Apol, G. Brancato, and A. Di Nola. Theoretical equations of state for temperature and electromagnetic field dependence of fluid systems, based on the quasi-gaussian entropy theory. *J. Chem. Phys.*, 116(11):4437–4449, 2002.

[70] M. D'Alessandro, M. D'Abramo, G. Brancato, A. Di Nola, and A. Amadei. Statistical mechanics and thermodynamics of simulated ionic solutions. *J. Phys. Chem. B*, 106:11843–11848, 2002.

[71] M. D'Abramo, M. D'Alessandro, and A. Amadei. On the use of the quasi-gaussian entropy theory in the study of simulated dilute solutions. *J. Chem. Phys.*, 120(11):5226–5234, 2004.

[72] F. Noè, I. Daidone, J.C. Smith, A. Di Nola, and A. Amadei. Solvent electrostriction-driven peptide folding revealed by quasi-gaussian entropy theory and molecular dynamics simulation. *J. Phys. Chem. B*, 112:11155–11163, 2008.

[73] A. Amadei, M.E.F. Apol, and H.J.C. Berendsen. Extensions of the quasi-gaussian entropy theory. *J. Chem. Phys.*, 106:1893–1912, 1997.

[74] M.E.F. Apol, A. Amadei, and H.J.C. Berendsen. On the use of the quasi-gaussian entropy theory in noncanonical ensembles. I. prediction of temperature dependence of thermodynamic properties. *J. Chem. Phys.*, 109(8):3004–3016, 1998.

[75] M.E.F. Apol, A. Amadei, and H. J.C. Berendsen. On the use of the quasi-gaussian entropy theory in non-canonical ensembles. II. prediction of density dependence of thermodynamic properties. *J. Chem. Phys.*, 109:3017–3027, 1998.

[76] H.J.C. Berendsen, J.P.M. Postma, W.F. van Gusteren, and Hermans J. *Intermolecular forces.* D. Reidel Publishing, Dordrecht, The Netherlands, 1981.

[77] H.J.C. Berendsen, J.R. Grigera, and T.P. Straatsma. The missing term in effective pair potentials. *J. Phys. Chem.*, 91:6269–6271, 1987.

[78] D.P. Tieleman and H.J.C. Berendsen. Molecular dynamics simulations of a fully hydrated dipalmitoylphosphatidylcholine bilayer with different macroscopic boundary conditions and parameters. *J. Chem. Phys.*, 105:4871, 1996.

[79] D. van der Spoel, P.J. van Maaren, and H.J.C. Berendsen. A systematic study of water models for molecular simulation: Derivation of water models optimized for use with a reaction field. *J. Chem. Phys.*, 108(24):10220–10230, 1998.

[80] D. van der Spoel, R. van Drunen, and H.J.C. Berendsen. Groningen machine for chemical simulations. Department of Biophysical chemistry, BIOSON Research Institute, Nijenborgh 4 NL-9717 AG Groningen, 1994.

[81] D. van der Spoel, A.R. van Buuren, E. Apol, P.J. Meulenhoff, D.P. Tieleman, A.L.T.M. Sijbers, R. van Drunen, and H.J.C. Berendsen. Gromacs user manual version 1.3. Nijenborgh 4, 9747 AG Groningen, The Netherlands, 1996.

[82] D.J. Evans and G.P. Morriss. *Statistical Mechanics of Nonequilibrium Liquids.* Academic, London, 1990.

[83] T. Darden, D. York, and L. Pedersen. Particle mesh ewald: An n $\cdot\log(n)$ method for ewald sums in large systems. *J. Chem. Phys.*, 98(12):10089–10092, 1993.

[84] M. Ratner and D. Ratner. *Nanotechnology: a gentle introduction to the next big idea.* Prentice Hall Press, Upper Saddle River, NJ, USA, 2002.

[85] C. P. Poole and F. J. Owens. *Introduction to nanotechnology.* John Wiley Sons. Inc., Hoboken, New Jersey, 2003.

[86] M. C. Roco. Nanotechnology: convergence with modern biology and medicine. *Current Opinion in Biotechnology*, 14(3):337–346, 2003.

[87] R. A. Freitas. What is nanomedicine? *Disease-a-Month*, 51(6):325–341, 2005.

[88] J. H. Park, S. Lee, J. Kim, K. Park, K. Kim, and I. C. Kwon. Polymeric nanomedicine for cancer therapy. *Prog. Polym. Sci.*, 33:113–137, 2008.

[89] H. Bader, H. Ringsdorf, and B. Schmidt. Water soluble polymers in medicine. *Angew. Makromol. Chem.*, 123/124:457–485, 1984.

[90] A. Harada and K. Kataoka. Switching by pulse electric field of the elevated enzymatic reaction in the core of polyion complex micelles. *J. Am. Chem. Soc.*, 125:15306–15307, 2003.

[91] N. Hedin, I. Fur, and P. O. Eriksson. Fast diffusion of the cl^- ion in the headgroup region of an oppositely charged micelle. a 35^{Cl} nmr spin relaxation study. *J. Phys. Chem. B*, 104(35):8544–8547, 2000.

[92] M. F. Ottaviani, R. Daddi, M. Brustolon, N. J. Turro, and D. A. Tomalia. Interaction between starburst dendrimers and sds micelles studied by continuous-wave and pulsed electron spin resonances. *Appl. Magn. Reson.*, 13(3-4):347–363, 1997.

[93] D. Bendedouch, S. H. Chen, and W. C. Koehler. Structure of ionic micelles from small angle neutron scattering. *J. Phys. Chem.*, 87(1):153–159, 1983.

[94] J. C. Earnshaw and E. McCoo. Surface light-scattering studies of surfactant solutions. *Langmuir*, 11(4):1087–1100, 1995.

[95] B. Lindman, N. Kamenka, M. C. Puyal, R. Rymden, and P. Stilbs. Micelle formation of anionic and cationic surfactants from fourier transform proton and lithium-7 nuclear magnetic resonance and tracer self-diffusion studies. *J. Phys. Chem.*, 88(21):5048–5057, 1984.

[96] H. J. C. Berendsen, D. van der Spoel, and R. van Drunen. Gromacs: A message-passing parallel molecular dynamics implementation. *Comput. Phys. Commun.*, 91:43–56, 1995.

[97] H. J. C. Berendsen, J. P. M. Postma, W. F. van Gunsteren, A. Di Nola, and J. R. Haak. Molecular dynamics with coupling to an external bath. *J. Chem. Phys.*, 81(8):3684, 1984.

[98] B. Hess, H. Bekker, H. J. C. Berendsen, and J. G. E. M. Fraaije. Lincs: A linear constraint solver for molecular simulations. *J. Comput. Chem.*, 18:1463–1472, 1997.

[99] A. D. MacKerell Jr. Molecular dynamics simulation analysis of a sodium dodecyl sulfate micelle in aqueous solution: Decreased fluidity of the micelle hydrocarbon interior. *J. Phys. Chem.*, 99:1846–1855, 1995.

[100] J. Bocker, J. Brickmann, and P. Bopp. Molecular dynamics simulation study of an n-decyltrimethylammonium chloride micelle in water. *J. Phys. Chem.*, 98:712–717, 1994.

[101] C. D. Bruce, M. L. Berkowitz, L. Perera, and M. D. E. Forbes. Molecular dynamics simulation of sodium dodecyl sulfate micelle in water: Micellar structural characteristics and counterion distribution. *J. Phys. Chem. B*, 106:3788–3793, 2002.

[102] C. D. Bruce, S. Senapati, M. L. Berkowitz, L. Perera, and M. D. E. Forbes. Molecular dynamics simulation of sodium dodecyl sulfate micelle in water: The behavior of water. *J. Phys. Chem. B*, 106:10902–10907, 2002.

RINGRAZIAMENTI

Approfitto di questa occasione per ringraziare tutte le persone che mi sono state vicine in questi tre anni del Dottorato di Ricerca.

In particolare il Prof. Alfredo Di Nola e il Dr. Andrea Amadei, che sempre disponibili, mi hanno guidato in questo lavoro con la loro grande competenza.

Ringrazio la dott.ssa Laura Zanetti Polzi, che oltre ad essere un'amica, é stata un'ottima collega di lavoro pronta ad aiutarmi e consigliarmi.

Il Dr. Paolo Marracino con cui ho condiviso gran parte di questo lavoro di ricerca.

Ringrazio, inoltre, tutte le persone del laboratorio.

Infine, un ringraziamento particolare ad una persona molto speciale.